



Competing Molecular Packing of Blocks in a Lamella-Forming Carbohydrate- block -poly(3-hexylthiophene) Copolymer

Yoko Sakai-Otsuka, Yoshiharu Nishiyama, Jean-Luc Putaux, Martin Brinkmann, Toshifumi Satoh, Wen-Chang Chen, Redouane Borsali

► To cite this version:

Yoko Sakai-Otsuka, Yoshiharu Nishiyama, Jean-Luc Putaux, Martin Brinkmann, Toshifumi Satoh, et al.. Competing Molecular Packing of Blocks in a Lamella-Forming Carbohydrate-block -poly(3-hexylthiophene) Copolymer. *Macromolecules*, 2020, 53 (20), pp.9054-9064. 10.1021/acs.macromol.0c01801 . hal-03075544

HAL Id: hal-03075544

<https://cnrs.hal.science/hal-03075544>

Submitted on 16 Dec 2020

HAL is a multi-disciplinary open access archive for the deposit and dissemination of scientific research documents, whether they are published or not. The documents may come from teaching and research institutions in France or abroad, or from public or private research centers.

L'archive ouverte pluridisciplinaire **HAL**, est destinée au dépôt et à la diffusion de documents scientifiques de niveau recherche, publiés ou non, émanant des établissements d'enseignement et de recherche français ou étrangers, des laboratoires publics ou privés.

Competing Molecular Packing of Blocks in Lamella-forming Carbohydrate-*block*-Poly(3-hexylthiophene) Copolymer

Yoko Sakai-Otsuka,¹ Yoshiharu Nishiyama,¹ Jean-Luc Putaux,¹ Martin Brinkmann,²

Toshifumi Satoh,³ Wen-Chang Chen,⁴ and Redouane Borsali^{1}*

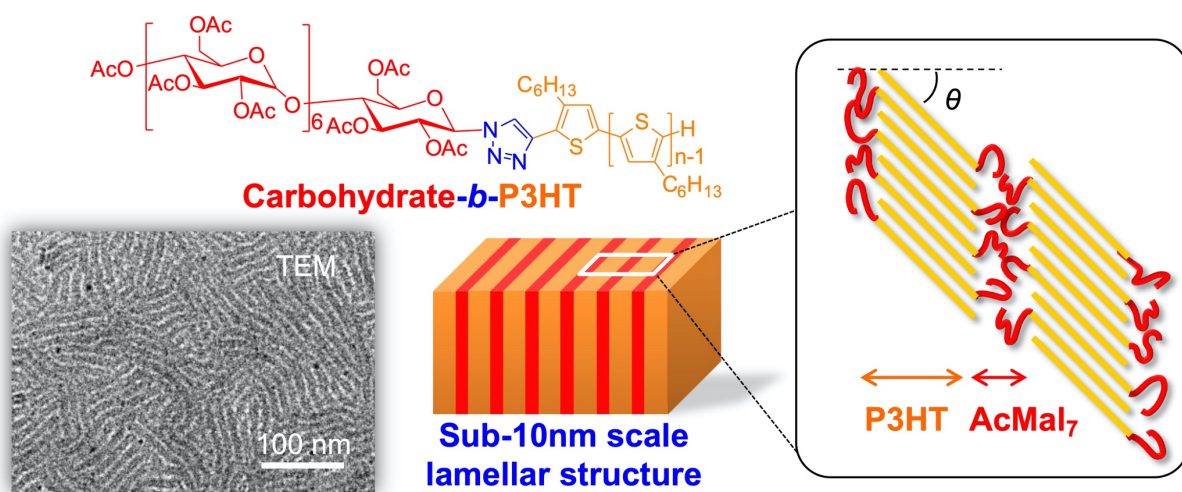
1) Univ Grenoble Alpes, CERMAV, CNRS, F-38000 Grenoble, France

2) Université de Strasbourg, CNRS, ICS UPR 22, F-67000 Strasbourg, France

3) Laboratory of Polymer Chemistry, Division of Applied Chemistry, Faculty of Engineering, Hokkaido University, N13W8, Kita-ku, Sapporo 060-8628, Japan.

4) Advanced Research Center for Green Materials Science and Technology, National Taiwan University, Taipei 10617, Taiwan

for Table of Contents use only



ABSTRACT

A molecular packing model of poly(3-hexylthiophene)-*block*-peracetylated maltopheptaose (P3HT-*b*-AcMal₇) was proposed based on the X-ray and electron diffraction measurements. The P3HT and AcMal₇ segments are confined in the lamellae in which the AcMal₇ segments are aligned side-by-side. The extended P3HT chain segments are tilted with respect to the lamellae plane and strongly π -stacked. This molecular arrangement results from a subtle balance between segregation strength of the P3HT and AcMal₇ blocks, strong π - π interactions of the P3HT backbones, geometrical mismatch between two blocks, space filling requirement and entropic penalties. The small-angle X-ray scattering (SAXS) analysis above the melting temperature of P3HT block indicates a strong segregation strength between P3HT and AcMal₇ blocks. Differential scanning calorimetry (DSC), Fourier-transform infrared spectroscopy (FT-IR) and SAXS measurements underline the improved thermal stability of P3HT crystalline domains in the phase-separated P3HT-*b*-AcMal₇.

INTRODUCTION

Block copolymers containing π -conjugated semiconducting polymers have attracted attention at the frontier of polymer chemistry and optoelectronic engineering due to their exceptional physical properties and wide structural tunability.^{1,2} They possess high potential for applications in optoelectronic technology including low-cost and flexible organic photovoltaic devices. In the past decade, the external power conversion efficiencies (EPCEs) of single junction donor-acceptor (D/A) bulk-heterojunction (BHJ) solar cells has continuously improved, reaching 14 %³ owing mostly to the development of new materials, such as *p*-type low-band-gap conjugated polymers^{4,5} and non-fullerene acceptors.⁶ While a large variety of promising materials have been reported,

morphology control of the BHJ blend at multiple length scales remains another central quest in the field. For instance, at the nanometer scale, the electron donating and accepting materials must be uniformly interfaced over the whole active layer (typically in form of lamella), ideally with each domain size compatible to the exciton diffusion length (10-15 nm), to guarantee that generated excitons reach the donor-acceptor interface within their lifetime prior to radiative and/or non-radiative decays.⁷ At the molecular scale, the crystal structure of semiconducting compounds must be optimized to get efficient charge carrier transport. Furthermore, morphological instability of the simply-blended BHJ impacts the long-term device performance. The self-assembly of π -conjugated block copolymers is an alternative and promising bottom-up strategy to meet these prerequisites. Among the wealth of conjugated polymers synthesized so far, regioregular poly(3-alkylthiophene) (P3AT) have been extensively employed as an electrically active polymer block due to their well-balanced characteristics such as optoelectronic properties, thermal and environmental stability, and synthetic accessibility.⁸⁻¹⁶ In particular, regioregular poly(3-hexylthiophene) (P3HT) has been the working horse of p-type semiconducting polymers. A variety of reports on the P3HT-based block copolymers can be found in the literature,⁸⁻¹⁵ but in most cases, strong π - π interactions of P3HT chains dominate over microphase separation. This results in a randomly-oriented nanofibril morphology,⁸⁻¹² which is often found in the P3HT homopolymer, irrespective of the volume fraction of each blocks. In this context, several research groups have attempted chemical modifications of alkyl side chain of P3ATs to weaken the rod-rod interaction between polythiophene backbones.¹⁷⁻²¹ For instance, Segalmen *et al.* reported the synthesis of poly(3-(2'-ethynyl)-hexylthiophene-*block*-polylactide) (P3EHT-*b*-PLA) bearing a bulkier branched alkyl side chain and successfully demonstrated various phase-separated structures including lamellae and cylinder depending on the volume fraction of the P3EHT block.¹⁸ This

enriched phase behavior was attributed to the introduction of a branching point in the side chain that results in a decrease of crystallization temperature of P3EHT. Whereas the P3EHT-*b*-PLA retained a good charge transport property comparable to the P3HT homopolymer, the low thermal stability of the block copolymers (melting point: P3HT (≈ 220 °C) \gg P3EHT-*b*-PLA (≈ 90 °C)) and less crystalline nature of the P3EHT may be detrimental for OPV applications. In this regard, the use of pristine P3HT as one of the blocks is important to exploit full potential of its characteristics.

With this mind, we have recently reported on the design and synthesis of a new class of carbohydrate-based block copolymer, poly(3-hexylthiophene)-*block*-peracetylated maltoheptaose (P3HT-*b*-AcMal₇), and demonstrated that the P3HT-*b*-AcMal₇ self-organized into a lamellar structure with a half-pitch of sub-10 nm that corresponds to the exciton diffusion length upon thermal annealing.²² The carbohydrate block was strategically introduced to impart a strong segregation strength to the block copolymer system, *i.e.* high Flory-Huggins interaction parameter χ , that arises from their chemical and steric imbalance between two blocks. In addition, the carbohydrate can be a sacrificial block because it can be removed by selective etching with acidic or basic medium. The resulting cavity would be eventually filled with electron acceptors to realize a nanostructured D/A morphology. It is interesting to note that rod-coil block copolymer systems containing π -conjugated polymer block such as the P3HT, the phase behavior is more complex than that of classical coil-coil block copolymer systems. Two additional parameters, the Maier-Saupé interaction (μN) and the conformation asymmetry (ϵ), should be taken into account in addition to the segregation strength parameter (χN) and the volume fraction of the segment. These two additional parameters often affect boundaries of the phase diagram. For instance, Olsen et al.²³ investigated self-assembly of a conjugated rod-coil block copolymer (PPV-*b*-PI) and reported a

universal phase diagram for the rod-coil block copolymers. According to the study, lamellar phases occupy a very large region in the phase diagram with a coil fraction up to 0.8, which is considerably a broader range than in classical block copolymers, most likely due to the strong rod-rod interaction. As will be described below, the value of 0.65 (the volume fraction of the P3HT in the P3HT-*b*-AcMal₇) fits within the range of lamellar phase in this specific rod-coil block copolymer system. Although our previous work has highlighted the great potential of the P3HT-*b*-AcMal₇, several aspects relative to the copolymer structuring needed further investigations.

Importantly, the crystallinity of constituent semiconducting materials has a significant impact on the device performance because it determines their charge transport properties.^{24,25} The orientation and crystalline structure of the semiconducting segments must be optimized to the practical use and must be controlled simultaneously with phase separation of block copolymers. Such organization is predominantly governed not only by the molecular properties but also by the processing conditions.²⁶ Hence, the knowledge of the detailed molecular packing of the P3HT block and its variation in the course of post-treatment are important aspects to investigate in order to attain a precisely-controlled model structure.

In this paper, we extend our previous study on self-assembly of carbohydrate-based block copolymers²² to gain further insight into the internal structure of the self-assembled P3HT-*b*-AcMal₇ and the self-assembly behavior upon thermal treatment. A comprehensive study on the thermally-induced structural evolution of the P3HT-*b*-AcMal₇ was carried out by *in situ* small- and wide-angle X-ray scattering (SAXS/WAXS) analysis with step-wise heating and cooling. The X-ray scattering were carefully interpreted together with the data from differential scanning calorimetry (DSC) and Fourier-transform infrared spectroscopy (FT-IR).

EXPERIMENTAL SECTION

Materials. Maltoheptaose was purchased from Nagase & Co., Ltd. (Japan) and all other reagents were purchased from Sigma-Aldrich and used as received without further purification unless otherwise specified. Peracetylated azido-functionalized maltoheptaose (AcMal₇-N₃) was synthesized as previously described.²² Regioregular alkyne-terminated poly(3-hexylthiophene) (alkyne-P3HT) was prepared by post-functionalization modification of Br/H-terminated P3HT via Stille coupling between Br-terminated polymer end with ethynyltributylstannane. The obtained mono-ethynyl-capped P3HT (SEC: $M_w = 6210 \text{ g mol}^{-1}$, $M_n = 5670 \text{ g mol}^{-1}$, $D = 1.07$; HT-HT regioregularity: > 95 %) was coupled with AcMal₇-N₃ through copper-catalyzed azide-alkyne cycloaddition (CuAAC "click" reaction) to afford poly (3-hexylthiophene)-*b*-peracetylated maltoheptaose (P3HT-*b*-AcMal₇) (volume fraction of P3HT: 0.65). The detailed synthetic procedures and characterization of the products are available in the supporting information.

Instruments. ¹H (400 MHz) and ¹³C (100 MHz) NMR spectra were recorded using a Bruker Avance DRX 400 MHz. FT-IR spectra were recorded using a Perkin-Elmer Spectrum RXI FT-IR Spectrometer. Size exclusion chromatography (SEC) was performed at 30 °C using an Agilent 390-MDS system (290-LC pump injector, ProStar 510 column oven, 390-MDS refractive index detector) equipped with Knauer Smartline UV detector 2500 and two Agilent PLgel 5μm MIXED-D 300 x 7.5 mm columns (Part No: PL1110-6504) in THF at the flow rate of 1.0 mL min⁻¹. DSC analysis was performed using a TA Instruments DSC Q200 equipped with RCS 90 cooling unit. The samples (*ca.* 5 mg) were firstly dissolved in THF and deposited on the aluminum DSC pan followed by slow evaporation of the solvent. These DSC samples were stored at 100 °C under vacuum for several hours prior to analysis. The measurements were carried out under a nitrogen

atmosphere at a scan rate of 10 °C min⁻¹. AFM phase images were recorded in tapping mode using a Picoplus microscope (Molecular Imaging, Inc., Tempe, AZ). Transmission electron microscopy (TEM) images and electron diffraction (ED) patterns of the spin-coated thin films were recorded using a CM200 Philips microscope (Hillsboro, OR, USA) operating at 200 kV equipped with a TVIPS F216 TemCam camera. The oriented thin films were observed by TEM at 120 kV in bright field (BF) and ED modes using a CM12 Philips microscope equipped with a MVIII (Soft Imaging System) Charge Coupled Device camera. SAXS and WAXS analyses were performed on the BM02 beamline D2AM at the European Synchrotron Radiation Facility (ESRF, Grenoble, France). X-rays of 18 keV ($\lambda = 0.6888 \text{ \AA}$) with a spot size of 100 μm were used for all the measurements. Scattering patterns were recorded on two photon-counting pixel detectors (WOS and D5 from imXpad). Power spectra of selected images were calculated using the ImageJ software.

Thin film preparation by mechanical rubbing and structural analysis.

About 30nm-thick films of P3HT-*b*-AcMal₇ were prepared by doctor blading from solutions in chloroform (5 wt % solution) on clean glass substrates. Mechanical rubbing of the copolymer films was performed following the methodology described in previous work.^{27–29} The rubbing temperature was adjusted between ambient and 200 °C. Two rubbing cycles were used. The alignment of the P3HT blocks was probed by polarized UV-vis absorption spectroscopy using a Cary 5000 spectrometer. Optimal alignment was observed for films rubbed at 190 °C. For TEM analysis, the copolymer films were first coated with an evaporated amorphous carbon film (Edwards Auto 306 evaporator). The samples were recovered from the glass substrate by the polyacrylic acid (PA) (20wt% aqueous solution, Aldrich). In brief, a droplet of PA is deposited on the carbon-coated film and left to dry for 3 hours. The dried PA with the film is stripped off from

the glass substrate using a razor blade and deposited on distilled water to dissolve PA. The carbon-coated films are then recovered on TEM copper grids.

RESULTS AND DISCUSSION

Synthesis of P3HT-*b*-Carbohydrate Diblock Copolymer via Modified Synthetic Route and its Self-Assembly in the Solid State. The P3HT-*b*-AcMal₇ diblock copolymer was synthesized in a similar way as described in the previous report except for the preparation of the alkyne-functionalized P3HT block (**Figure 1a**).²² In the previous study, an *in situ* end-functionalization was used to prepare regioregular alkyne-P3HT.²² However, this method yields P3HTs with a small amount of high molecular weight impurities possibly due to alkyne-alkyne homocoupling between reactive ethynyl-capped P3HTs during the end-capping process. To circumvent these undesirable by-products which may affect the morphology of the self-assembled block copolymer film, an alternative synthetic route based on a post-polymerization modification method was applied.²⁹ The selective ethynyl-functionalization onto the Br-terminal of the stable precursor polymer resulted in a remarkable reduction of the production of dimerized P3HT and a small 1.07 polydispersity index \bar{D} (see Supporting Information **Figure S1**). All the synthetic details and characterization data are available in the supporting information. The self-assembly behavior of the newly synthesized P3HT-*b*-AcMal₇ showed almost the same trend as the previous one²² except for the domain size. Both samples self-organized into well-defined lamellar structures upon thermal heating when the block copolymers obtained enough mobility to reach the equilibrium state (**Figures 1b** and **S3**). On the one hand, the *d*-spacing of the new sample estimated from the power spectrum of the TEM images was found to be *ca.* 12 nm which is slightly smaller than that of the block copolymer synthesized by the previous method (*ca.* 14 nm) (**Figure S3**) that had the same

molecular weight. The difference in *d*-spacing was further supported by SAXS analysis, showing the *d*-spacing of 12.2 nm for the new sample and of 15.4 nm for the previous sample (**Figures 1d** and **S3**). This deviation is most likely attributed to the amount of dimerized P3HT in the block copolymer sample (**Table S2**). The ED pattern of the new sample indicates that the P3HT segments form crystalline domains by showing a diffraction ring attributable to the π - π stacking of the P3HT backbone corresponding to a spacing of *ca.* 0.38 nm (**Figure 1c**).

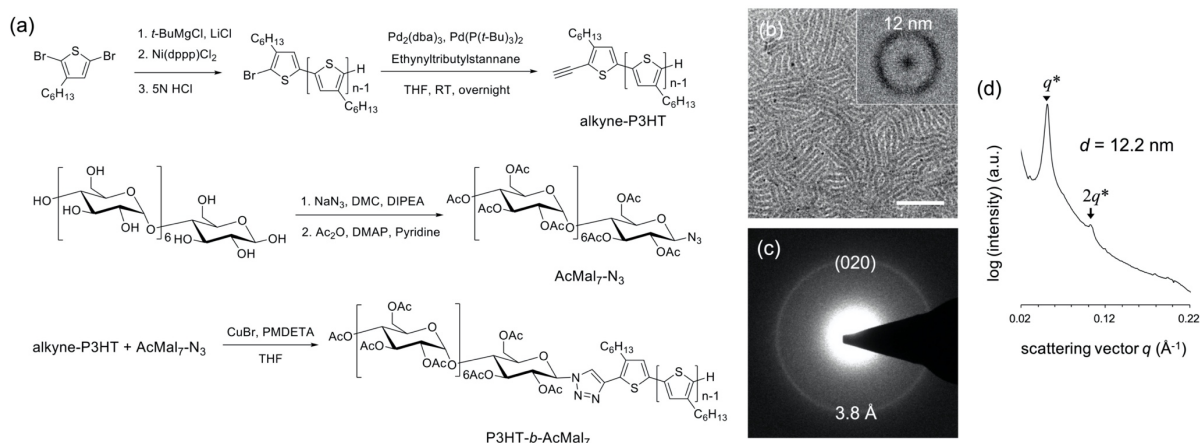


Figure 1. (a) Synthetic route of P3HT-*b*-AcMal₇ diblock copolymer. (b) TEM image of the P3HT-*b*-AcMal₇ thin film obtained after thermal annealing at 220 °C for 10 min. Scale bar indicates 100 nm. Inset: Power spectrum of the image. (c) Electron diffraction pattern of the phase-separated P3HT-*b*-AcMal₇ thin film showing a diffraction ring corresponding to the π - π stacking of the P3HT backbone with 0.38 nm. (d) SAXS profile of the P3HT-*b*-AcMal₇ bulk sample after thermal annealing at 220 °C for 10 min.

Molecular Packing Model. In the present case where the lamellar structure is built up with A-B type diblock copolymers, the following three models depicted in **Figure 2** are possible: (a) monolayer packing with non-interdigitated AcMal₇ segments, (b) monolayer packing with interdigitated AcMal₇ segments, (c) a bilayer structure with a tail-to-tail packing of P3HT blocks

and non-interdigitated AcMal₇ segments. According to the SAXS measurements, the phase separation of the P3HT-*b*-AcMal₇ results in a 12.2 nm *d*-spacing of the lamellar structure. On the other hand, the *d*-spacing calculated from a broad primary scattering peak of the alkyne-P3HT homopolymer was found to be 10.7 nm, which is consistent with the average width of the P3HT nanofibers (**Figure S4**). Twice the length of the extended P3HT blocks in tail-to-tail configuration (c) amounts to 21.4 nm that exceeds largely the observed periodicity of 12.2 nm. Therefore, we can rule out the bilayer packing of the copolymer (c). Only the packing schemes (a) and (b) are a priori possible and will be discussed hereafter.

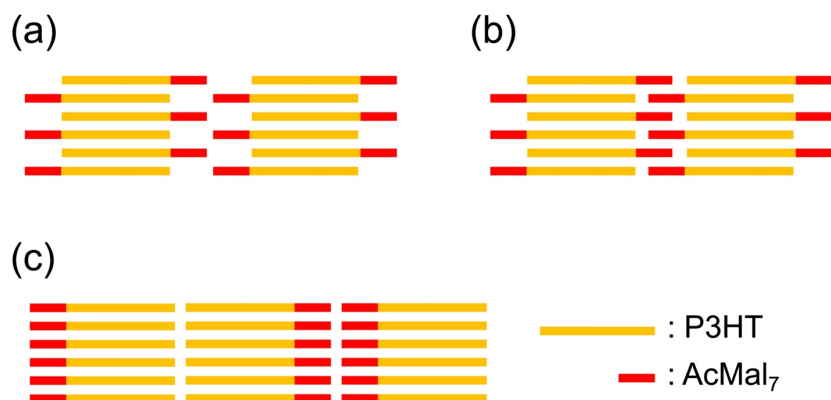


Figure 2. Schematic images of possible packing models for lamellar structure of the P3HT-*b*-AcMal₇, where orange and red bars represent the P3HT and AcMal₇ segments, respectively. (a) monolayer, non-interdigitated AcMal₇ packing (side-by-side arrangement), (b) monolayer, interdigitated AcMal₇ packing, and (c) bilayer, non-interdigitated AcMal₇ packing. For simplicity, scale and tilt of each block are disregarded here.

Since the P3HT and AcMal₇ blocks are tethered, they must share the same lateral arrangement. The cross-sectional areas (*A*) of the P3HT and AcMal₇ segments, which deservedly have an impact on the molecular conformation especially at the interface of the two blocks, were therefore estimated on the basis of the unit cell parameters (*a*, *b*, and γ) according to the following equation:

$$A = ab\sin(\gamma)/n \quad (1)$$

where n is the number of chains per unit cell. Since the peracetylated maltoheptaose does not contain enough glucose units, it does not form periodic helical structures observed for many other polysaccharides but may have an amorphous structure. Thus, alternatively, the unit cell parameters of amylose triacetate (form I) which has exactly the same chemical structure as AcMal₇, *i.e.* peracetylated linear α -1,4 linked D-glucan was used for the calculation.³¹ We suppose that this crystal structure is the most compact one for AcMal₇ in the solid state. The calculated cross-sectional areas of the P3HT (A_{P3HT}) and AcMal₇ (A_{AcMal_7}) are 0.62 and 1.03 nm², respectively (**Table 1**). The A_{AcMal_7} is found to be 1.7 times larger than the A_{P3HT} . Considering the fact that a diffraction ring attributable to the π -stacking of the thiophene backbone (*ca.* 0.38 nm) has been observed in the ED pattern of the phase-separated P3HT-*b*-AcMal₇ thin film (**Figure 1c**), the P3HT segments should have a crystalline structure closely similar to the unit cell reported for form I.³² In this case, the AcMal₇ segments cannot interdigitate each other due to their large molecular dimension compared with that of the P3HT segments. Therefore, the side-by-side arrangement (**Figure 2a**) seems the most likely model.

Table 1 Structural parameters of P3HT and AcMal₇

| | P3HT | AcMal ₇ |
|-----------------------------------|--|--|
| unit cell parameters ^a | $a = 1.60 \text{ nm}$ $b = 0.78 \text{ nm}$ $c = 0.78 \text{ nm}$ $\gamma = 86.5^\circ$ | $a = 1.09 \text{ nm}$ $b = 1.89 \text{ nm}$ $c = 5.39 \text{ nm}$ $\gamma = 90.0^\circ$ (amylose triacetate) |
| cross-sectional area | 0.62 nm ² | 1.03 nm ² |
| density ^a | 1.14 g cm ⁻³ | 1.20 g cm ⁻³ |

^a Unit cell parameters and density for P3HT and AcMal₇ were referred from ref. 32 and ref. 31, respectively.

Non-polar molecules tend to fill the space avoiding free volumes, to reduce the enthalpy. Now suppose that the AcMal₇ segments first form a stable structure analogous to the crystal structure of the model compound of amylose triacetate. If the P3HT segments are aligned parallel to the AcMal₇ segment without tilt as shown **Figure 3a**, the π - π stacking distance of the P3HT backbone would be determined by intermolecular distance of AcMal₇ of 1.09 nm because of the bulky structure of the AcMal₇. In this case, the predicted density of the P3HT segment for this arrangement ($\rho_{\text{P3HT, EX}} = 0.77 \text{ g cm}^{-3}$) is considerably lower than that of the crystal ($\rho_{\text{P3HT, crystal}} = 1.14 \text{ g cm}^{-3}$),³¹ indicating that the non-tilted P3HT arrangement is thermodynamically unfavorable. In order to maintain the crystal density, the P3HT should be stacked with a stacking period of 0.78 nm per two chains equivalent to the lattice parameter b . Hence, the tilting of the P3HT main chain is the only solution compatible with a thermodynamically stable packing. The structure in consideration of the consistency with the crystal density is presented in **Figure 3b**. The tilt angle based on this model can be estimated as follows:

$$\theta \approx \arccos (0.78 \text{ nm}/1.09 \text{ nm}) \approx 44^\circ$$

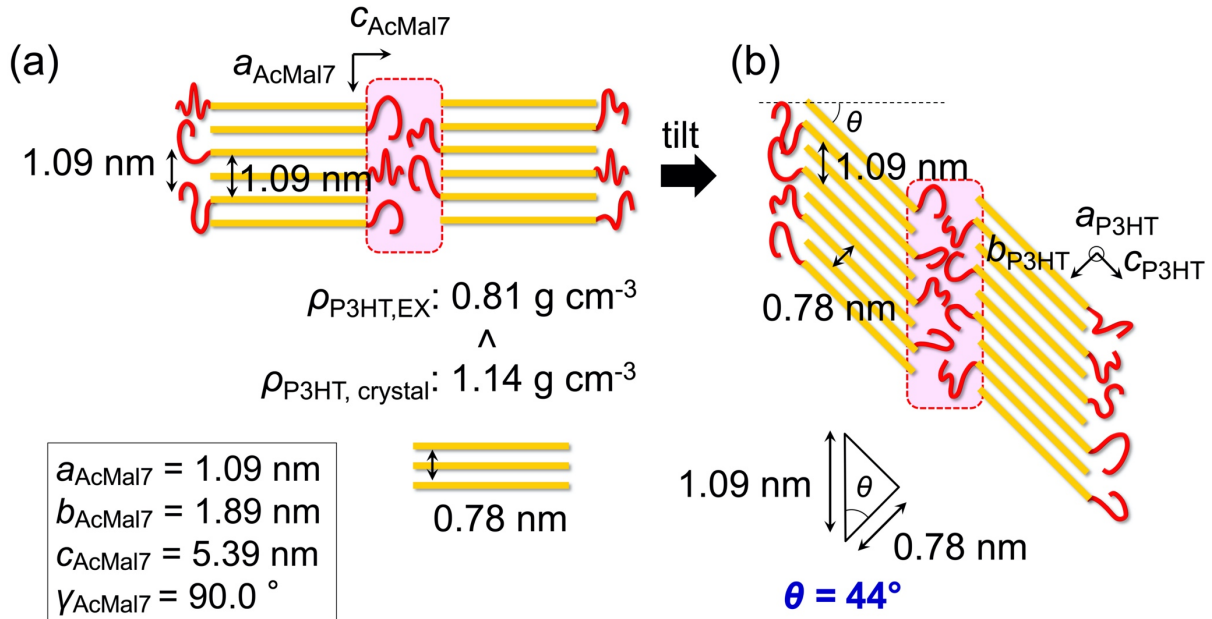


Figure 3. Schematic illustrations of (a) hypothetical arrangement and density assuming P3HT segments are aligned parallel to the AcMal₇ segments, and (b) expected arrangement estimated based on space-filling density argument. Orange and red lines represent the P3HT and AcMal₇ segments, respectively.

To further assess the tilt arrangement based on space-filling arguments, additional ED measurements were performed on a highly oriented P3HT-*b*-AcMal₇ film. A uniform alignment of the lamellar structure over large area was achieved by high-temperature rubbing and allowed for a precise evaluation of the tilt angle of the P3HT backbone with respect to the lamellar plane. Rubbing is particularly effective to prepare alignment layers in the field of display technology³³ and to orient semiconducting polymers such as P3HT.^{28,29,34} Rubbing P3HT-*b*-AcMal₇ at 190 °C afforded a highly oriented lamellar structure as shown in **Figure 4a**. The TEM image of the rubbed film reveals a preferential perpendicular alignment of the lamellar structure to the rubbing direction. A 12.5 nm lamellar periodicity was estimated from the FFT of the TEM image. It is identical to that measured for the annealed thin films prepared by spin-coating. The ED pattern of the rubbed film is shown in **Figure 4b**. The absence of the (*h*00)_{P3HT} reflections implies no "face-on" orientation, i.e. hexyl side chains of the P3HT align exclusively perpendicular to the substrate. The 020_{P3HT} reflection representing the π -stacking of the P3HT is observed with intense arcs at $\pm 57^\circ$ relative to the rubbing direction. The presence of the anisotropic intensity in the Scherrer ring forthrightly indicates $\pm 33^\circ$ tilting of the P3HT backbones with respect to the lamellar plane as illustrated in **Figure 4c**. This tilt between the rubbing direction R and the chain direction is further in agreement with the low values of the dichroic ratio measured by polarized UV-vis spectroscopy.

It is also noteworthy that for a homopolymer of equivalent M_n , c_{P3HT}/R , indicating that the $\pm 33^\circ$ tilt is a consequence of the presence of the AcMal₇ block.

From the above-mentioned considerations and experimental evidence obtained by ED, it can be concluded that the P3HT and AcMal₇ segments are confined in the lamellae in which the AcMal₇ segments are aligned side-by-side (no interdigitation). The P3HT segments are tilted about $33\text{--}44^\circ$ with respect to the lamellae plane and strongly π -stacked with an extended chain conformation in order to attain thermodynamically stable crystalline structure. An overall view of the proposed molecular packing model for lamellar structure of P3HT-*b*-AcMal₇ is depicted in **Figure S5**.

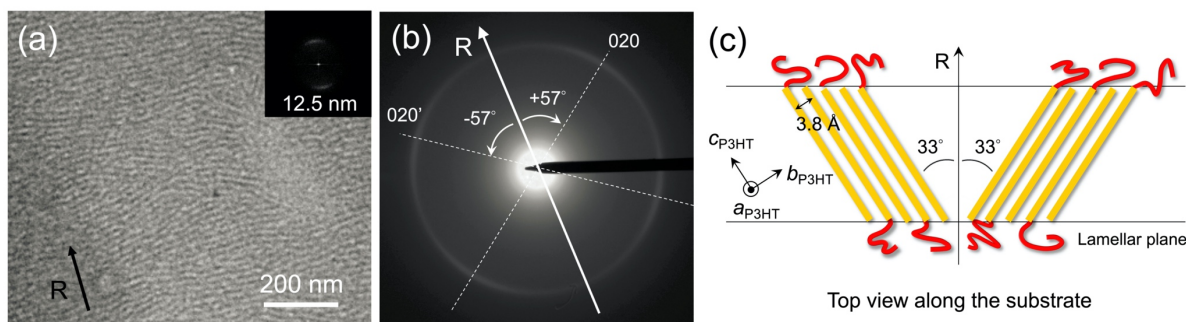


Figure 4. (a) TEM image of highly-oriented P3HT-*b*-AcMal₇ film prepared by high-temperature rubbing at 190 °C. (b) Electron diffraction pattern of the rubbed P3HT-*b*-AcMal₇ film. (c) Schematic illustration of the possible alignment of the P3HT block with a tilt angle of 33° . Orange and red lines represent the P3HT and AcMal₇ segments, respectively. The rubbing direction (R) is indicated by an arrow.

Role of the Temperature on the Structure.

a) Thermal Stability of the P3HT Crystals Confined in the Phase-Separated P3HT-*b*-AcMal₇.

Figure 5a shows DSC heating traces of the P3HT-*b*-AcMal₇ and alkyne-P3HT samples

crystallized at a slow 2 °C min⁻¹ cooling rate. As seen in the previous study,²² an endothermic peak associated with the melting process of P3HT crystal of the P3HT-*b*-AcMal₇ was observed at higher temperature ($T_m = 194$ °C) than that of the P3HT homopolymer ($T_m = 188$ °C). The relation of the corrected melting enthalpy $\Delta H_{m,P3HT}$ for the respective polymers coincides with the order of T_m , P3HT-*b*-AcMal₇ (18.9 J g⁻¹) > alkyne-P3HT (15.5 J g⁻¹). Note that the $\Delta H_{m,P3HT}$ were determined by integration of melting peak area followed by normalization by the weight fraction of P3HT in the sample to give the amount of heat per P3HT unit weight. These trends in the T_m and $\Delta H_{m,P3HT}$ indicate an enhanced stability of the crystalline P3HT domain confined in the phase-separated P3HT-*b*-AcMal₇ whereas the T_m and ΔH_m of many other phase-segregated rod-coil block copolymers were often reported lower than those of the constituent crystalline homopolymer due to a detrimental effect of non-crystalline coil-block on the crystalline perfection.^{12,35,36} This observation is further supported by temperature-dependent *in situ* FT-IR spectroscopy. According to the preceding study, the absorption bands in the 850-790 cm⁻¹ region are susceptible to the out-of-plane bending mode of the C β -H (see **Figure 5d**; related atoms are indicated in blue) on the thiophene ring ($\delta(C\beta-H)$). Particularly, the characteristic bands at 820 and 833 cm⁻¹ have been respectively assigned to the $\delta(C\beta-H)$ in the crystalline and in the amorphous phases.³⁷ Thus, both bands were used to monitor the crystalline state of the P3HT segment of the block copolymer. The whole absorption spectrum of the P3HT-*b*-AcMal₇ (4000-450 cm⁻¹) recorded at room temperature and the assignments of the characteristic bands are available in the Supporting Information (**Figure S6** and **Table S4**). **Figures 5b** and **5c** show variations of FT-IR absorption spectra of the P3HT-*b*-AcMal₇ in the 850-790 cm⁻¹ region during heating and cooling process, respectively. In the heating cycle, the band located at 820 cm⁻¹ decreases in intensity while the band at 833 cm⁻¹ becomes dominant. At 195 °C, the peak at 820 cm⁻¹ completely disappeared, meaning that the P3HT

segments are in the amorphous phase. In the cooling cycle, a reverse phase transition from amorphous to crystal is observed. A similar spectral change was observed in the P3HT homopolymer except that the temperature ranges where the phase transitions occurred were lower (**Figure S7**). In **Figure 5e**, the intensities at 820 cm^{-1} (A_{820}) are plotted as a function of increasing temperature to better visualize the structural change. With increasing temperature, an abrupt decrease of A_{820} is observed for both samples. However, the crystalline-to-amorphous phase transition of the homopolymer begins/completes at a temperature about $5\text{ }^{\circ}\text{C}$ lower than that of the P3HT-*b*-AcMal₇. These results provide another evidence to confirm the higher thermal stability of the P3HT crystalline structure in the P3HT-*b*-AcMal₇ organization.

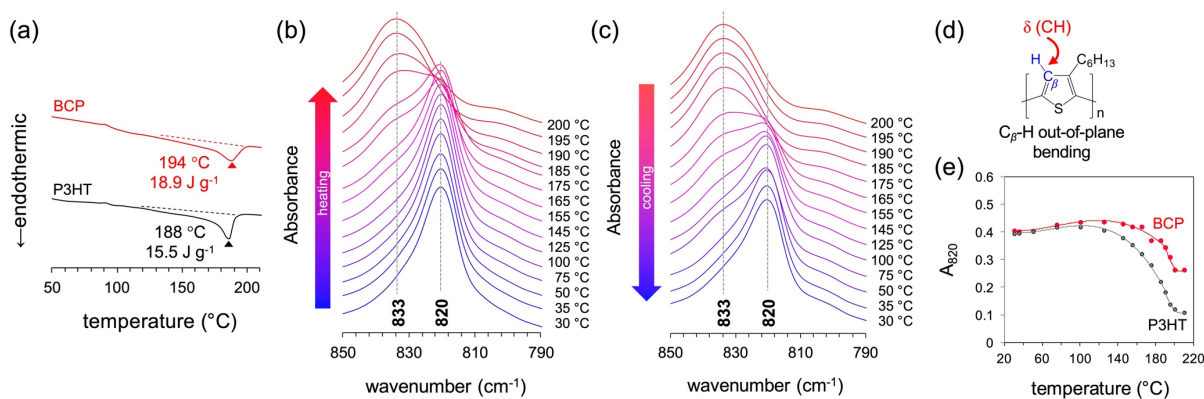


Figure 5. (a) DSC thermograms of P3HT-*b*-AcMal₇ (red) and alkyne-P3HT (black) recorded during heating cycle with a heating rate of $10\text{ }^{\circ}\text{C min}^{-1}$ after cooling with a cooling rate of $2\text{ }^{\circ}\text{C min}^{-1}$. Variation of FT-IR absorption spectra of P3HT-*b*-AcMal₇ in the region of C_β-H out-of-plane deformation associated with π -stacking mode of thiophene rings during (b) heating and (c) cooling process. (d) Chemical structure of P3HT. The atoms related to the C_β-H out-of-plane bending mode are indicated in blue. (e) Absorption intensity at 820 cm^{-1} of the corresponding FT-IR spectra of P3HT-*b*-AcMal₇ (red) and P3HT (black) during the heating process as a function of temperature.

b) Effect of Crystallization Rate on the Melt Behavior of P3HT-*b*-AcMal₇

Figures 6a and **6b** show the DSC thermograms of P3HT-*b*-AcMal₇ and alkyne-P3HT, respectively. The thermograms correspond to the heating cycles (heating rate of 10 °C min⁻¹) recorded after a cooling process from 220 to 0 °C. The cooling was realized at different cooling rates in the range 2-30 °C min⁻¹. The melting enthalpy based on the total sample weight ($\Delta H_{m, \text{total}}$) and corrected melting enthalpy ($\Delta H_{m, \text{P3HT}}$) were determined from each thermograms. The detailed data are summarized in the **Table S5**. For all heating traces of the P3HT homopolymer, a single endothermic peak corresponding to the T_m of the P3HT segment was observed. The value of T_m is insensitive to the cooling rate. On the other hand, in a series of heating traces of the P3HT-*b*-AcMal₇, an obvious change in the melting behavior was found depending on the cooling rate. In the first heating run and second heating run after underwent the slow crystallization (cooling rate of 2 °C min⁻¹), a single endothermic peak was observed around 193-194 °C. When the sample was crystallized at a higher cooling rate, an additional endothermic peak appeared in the heating scans. For example, for a cooling rate of 10 °C min⁻¹, two melting peaks were observed at 190 and 198 °C. With the increase of the cooling rate, the former peak was shifted to lower temperature from 190 to 186 °C, whereas the later peak remained at the same position. This observation implies that there are at least two crystalline states which are formed through different crystallization process, *i.e.* the lower- T peak corresponds to the crystallization governed by kinetic factor and the higher- T peak corresponds to the crystallization governed by thermodynamic factor. If the crystallization rate is fast enough, the crystallization behavior may be governed by thermodynamic factor and is not susceptible to the cooling rate. On the contrary, if the crystallization rate is very slow, with increasing cooling rate, kinetic factor becomes dominant and it results in less ordered semi-crystalline structures because of an insufficient time to crystallize into thermodynamically stable

equilibrium structure. Therefore, it is reasonable to assume that the crystallization of the P3HT-*b*-AcMal₇ system takes place via two processes: slow and fast crystallization. The existence of these multi-crystallization processes might reflect the different environments for the P3HT segment in the P3HT-*b*-AcMal₇ melt, *i.e.*, chain-end tethered with AcMal₇ (low mobility, modest steric hindrance), middle part (highly crystalline part), and free chain-end (high mobility), etc.

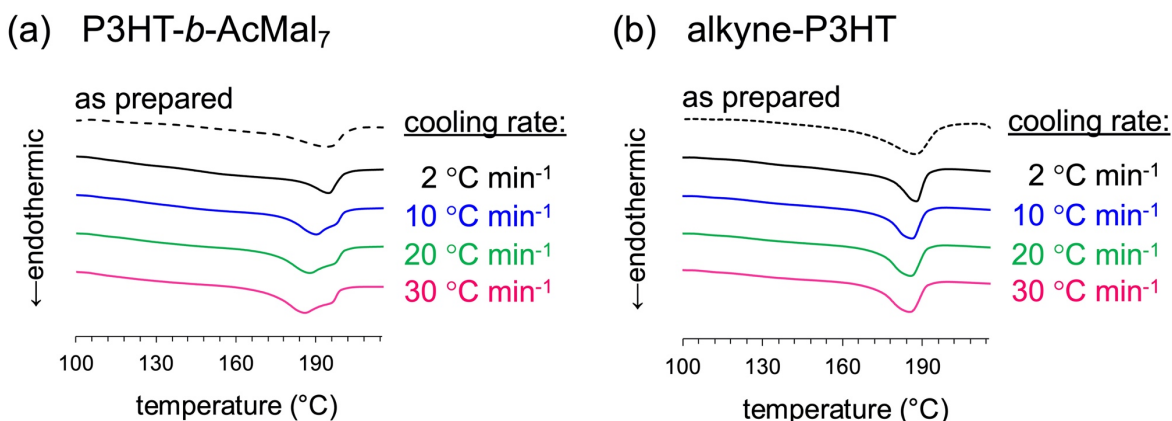


Figure 6. DSC thermograms of (a) P3HT-*b*-AcMal₇ and (b) alkyne-P3HT recorded during heating cycles with a heating rate of 10 °C min⁻¹ after cooling cycle with different cooling rate.

c) *In situ* Evaluation of Thermally-Induced Micro-Phase Separation of the P3HT-*b*-AcMal₇ by Small-angle X-ray Scattering Analysis. To investigate the temperature dependence of the micro-phase separation in detail, an *in situ* SAXS analysis during the heating and cooling was performed on the bulk sample of the P3HT-*b*-AcMal₇ (**Figures 7a** and **7b**). The bulk samples were stepwise heated from room temperature to 230 °C with an interval of 10 °C and then cooled below 100 °C by simple heat dissipation. As shown in **Figure 7a**, the SAXS profiles below 120 °C show no clear diffraction compared to the central scattering. At 130 °C, two peaks originated from the micro-phase separation (indexed as q^* and $2q^*$) appeared in a q -range between 0.04 and 0.13 Å⁻¹ and progressively become intense and sharper as the temperature increases. Then, above 188 °C,

a drastic sharpening of the q^* and $2q^*$ peaks is observed. These sharply-defined peaks are sustained in the initial stage of cooling process between 210 to 180 °C, then become broader. At the same time, a broad peak indexed as the 100 reflection, corresponding to the interlayer distance separated by the hexyl side chain, is also observed in a higher q -range. As the temperature increases, the 100 peak became sharper and shifted toward lower q region. The shift is due to thermal expansion of the hexyl side chains, and the sharpening reflects an increasing long-range order. The same thermal behavior is found for the 100 reflection of the P3HT homopolymer expect for the fact that the 100 peak of homopolymer vanishes at 200 °C (**Figure S8**) whereas that of the block copolymer remains up to 220 °C. Again, this indicates that a higher temperature is required to melt the P3HT crystalline structure when AcMal₇ is attached to the P3HT segment. In the cooling processes from the molten state, 100 reflection peak of the P3HT-*b*-AcMal₇ and the homopolymer appear again at 180 and 150 °C, respectively. Upon further cooling, the 100 peak shifts back toward its original position while the peak broadens. The broadening of the 100 peak during the cooling is counter-intuitive but the shrinking of the hexyl groups might have introduced internal strain. The detailed discussion about the crystal structure of the P3HT segment will be described later sub-section.

Herein, it is interesting to observe that the P3HT-*b*-AcMal₇ system displays well-ordered lamellar structure in the molten state, which can be assimilated to liquid crystals or phase separation of flexible polymers. This is a direct evidence that the P3HT-*b*-AcMal₇ possesses a strong segregation strength (χN) between P3HT and AcMal₇ segments. In the crystalline-rubber block copolymer system whose T_c is in between the order-disorder temperature (T_{ODT}) and T_g ($T_{ODT} > T_c > T_g$), crystallization precedes solidification of rubber block upon cooling. Hence, when the segregation strength between crystalline and rubber blocks is not sufficiently high, microphase-separated

structure formed in the molten state will be destroyed due to the strong crystallization tendency of the crystalline block.³⁸ In strong contrast, we observe that the crystallization of the P3HT segments of P3HT-*b*-AcMal₇ takes place within the phase-separated nanodomains of the lamellar phase, indicating that P3HT and AcMal₇ are strongly segregated throughout the whole structure formation process.

The variation of *d*-spacing of the lamellar structure calculated from the q^* peak position is shown in **Figure 7c**. Throughout the entire process, three obvious transitions, that can be linked to the thermal properties of the two blocks, are observed. Firstly, in the vicinity of the glass transition of the AcMal₇ ($T_{g, \text{AcMal}_7, \text{offset}} = 120 \text{ }^\circ\text{C}$), a characteristic peak q^* appeared. With the temperature increases up to 175 °C, the corresponding *d*-spacing gradually increases from 11.7 to 12.6 nm. As evidenced by DSC and temperature-dependent FT-IR measurements, in this temperature range, the AcMal₇ and P3HT segments gain mobility and exhibited the structural change. Hence, it is reasonable to assume that the block copolymer experienced a rearrangement as a consequence of relaxations of the AcMal₇ and P3HT segments from the collapsed state which was initially induced by rapid solvent evaporation during sample preparation. Secondly, above 175 °C where the P3HT block is partially molten, i.e. above the onset temperature of the melting area ($T_{m, \text{P3HT-}b\text{-AcMal}_7, \text{onset}}$), the *d*-spacing shows a sudden downward trend due to a shrinkage of the P3HT in molten state and can be at least attributed to decreasing segregation strength. Thirdly, in the cooling cycle, the *d*-spacing increases monotonically in the temperature range between 220 and 150 °C where the P3HT segment is in a molten state (above $T_{c, \text{P3HT-}b\text{-AcMal}_7, \text{onset}}$) but the segment becomes more extended up to the fully extended state in the crystals. After the P3HT segment is crystallized, the *d*-spacing shows a small declining trend with the temperature decrease probably due to the thermal contraction of the existing lamellae. It is worth noting that in the cooling process, a linear

dependence of d -spacing versus $1/T$ was always reported for the coil-coil block copolymer melts under the T_{ODT} .³⁹ In our rod-coil system, the shrinkage in d -spacing with reduced temperature during the cooling process below 150 °C was observed. This could be caused by the more compact π - π stacking of crystallized P3HT segments under lower temperatures. Similar conclusion, the increased packing density of P3HT segments under a reduced temperature, was also reported in simulation study.⁴⁰

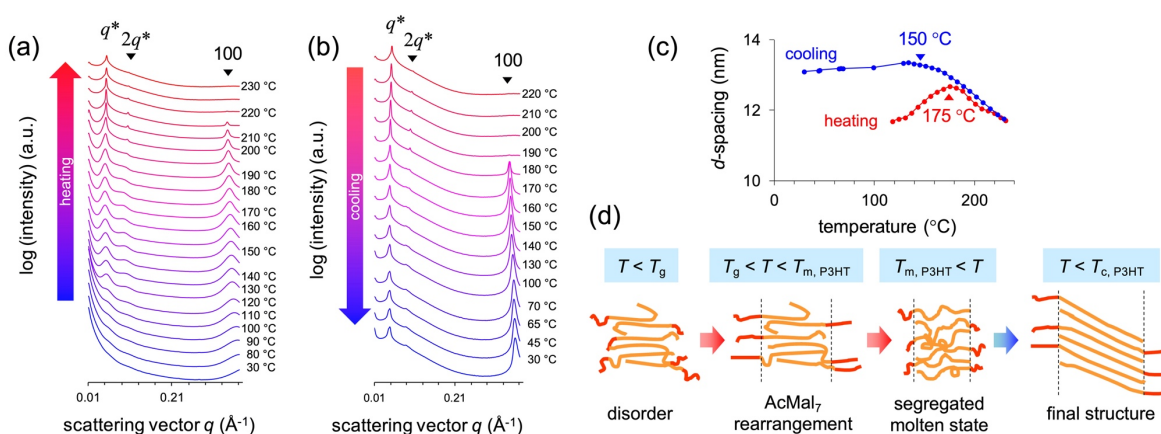


Figure 7. SAXS profiles of P3HT-*b*-AcMal₇ bulk sample taken during *in situ* (a) heating process from 30 to 230 °C and (b) cooling process from 220 to 30 °C. (c) Temperature dependence of the d -spacing of P3HT-*b*-AcMal₇ lamellae during *in situ* measurement. (d) Schematic illustration of possible conformational changes over thermal processing, where orange and red lines represent P3HT and AcMal₇ segments, respectively. The relative size of each block is disregarded here.

d) *In situ* Evaluation of Crystalline Structure of the P3HT-*b*-AcMal₇ by Temperature-Dependent Wide-angle X-ray Scattering Analysis. The black profile in Figure 8a shows the diffraction pattern of as-prepared bulk sample of the P3HT-*b*-AcMal₇. Three distinct diffraction peaks are observed in the q -range from 0.6 to 2.1 Å⁻¹. These peaks are found in the vicinity of the reflection positions of the P3HT estimated based on the reported unit cell,³² indicating that the

P3HT synthesized in this study have a similar crystal structure to the reported unit cell of form I. Two intense reflections located below 1.20 \AA^{-1} can be indexed as 200 and 300 (periodicity along the hexyl side chain direction). The intense peak at 1.64 \AA^{-1} arises from the overlap of the 020 and 002 reflections and is dominated by the intense 020 (π - π stacking periodicity). After thermal annealing, the entire diffraction peaks became sharper and the peak positions shifted (red profile in **Figure 8a**). In other words, thermal annealing leads to not only larger apparent crystallite sizes but also changes the crystal lattice. Taking a close look at the change, the $h00$ reflections shifted toward lower q after thermal treatment. To be specific, the d -spacing of 200 peak increased from 8.02 to 8.50 \AA upon annealing, which corresponds to an expansion by 6% along the alkyl side chain direction. On the other hand, a broad reflection peak 020 centered at $q = 1.64 \text{ \AA}^{-1}$ shifted to a higher q -range region at around $q = 1.67 \text{ \AA}^{-1}$. This reflects a shrinking of the lattice spacing from 3.83 to 3.77 \AA that is equivalent to a reduction in size by 1.6 %. The similar structural changes of the P3HT homopolymer induced by temperature were reported by Pietsch⁴¹ and Grigorian.^{42,43} For a monoclinic system, this reduction can be due to either (i) shrinking of c -axis (i.e. chain shrinkage), (ii) reduction in the π -stacking distance (i.e. shortening of the b -axis) or (iii) change in the monoclinic angle. Since the backbone is quite rigid, and no explanation can be found to reduce the π -stacking distance with increased temperature, scenario (iii) seems to be the most probable. Molecularly it represents a shift between layers composed of π -stacked chains that can be induced by the change in the tilt angle of hexyl groups. In any case, the P3HT segment in the block copolymer experienced a structural transition from the crystal structure analogous to that of P3HT unit cell to thermodynamically more stable structure by adopting its crystal conformation to the phase-separated nano-domain in the course of thermal treatment.

Figure 8b presents the evolution of WAXS profiles during the heating process of the P3HT-*b*-AcMal₇. With the temperature increase up to 120 °C, the 020 peak slightly shifts toward higher q -range, which is opposite to the shift of $h00$ peaks, then shifts back to lower q by further heating above 120 °C. **Figures 8c** and **8d** show a variation of the d -spacing calculated from the peak position of 200 reflection (d_{200}) and one calculated from the peak position of 020 reflection (d_{020}), respectively, together with the first temperature derivatives of the corresponding d -spacing. The d_{200} follows a similar trend as d_{100} what is seen in **Figure 7a**, with a slow transition between 60 and 110 °C superimposed with a linear thermal expansion coefficient of about 800 ppm K⁻¹. The transition is accompanied by about 6 % increase in d_{200} . The d_{020} also shows a similar trend with a thermal expansion coefficient of 100 ppm K⁻¹ and the transition between 60 and 110 °C which induces a decrease of d -spacing of about 1 %. The first derivatives of d_{200} showed a close similarity in shape to that of d_{020} but with opposite sign, supporting the phase transition occurring between 60 and 110 °C.

The *in-situ* WAXS experiment revealed the difference between the annealed and as cast samples of P3HT-*b*-AcMal₇ comes from the phase transition occurring between 60 and 110 °C during the first heating, where the basic arrangement of P3HT segment slightly changes. This phase transition was not accompanied by a change in internal energy as no heat-flow could be detected in the DSC thermogram. If the d_{100} increased by 6 % and d_{020} shrank by 1 % during the phase transition, the net density of P3HT segments decreased which should lead to an increase in internal energy. This might have been compensated by the densification and rearrangement of AcMal₇ segment, which was not detectable by diffraction due to its amorphous nature. In the solution casting, the P3HT segment starts to crystallize prior to complete evaporation of the THF solvent, and the structure formation might be dictated by the crystallization tendency of P3HT leading the AcMal₇ in high-

energy packing situation. In the complete absence of solvent, the thermal annealing would soften the P3HT segments, allowing the AcMal₇ segment to relax, imposing some constraint on P3HT that converts into another crystalline form. The net enthalpy would be almost zero as the conversion is simply a transfer of internal energy from AcMal₇ segments to P3HT segments.

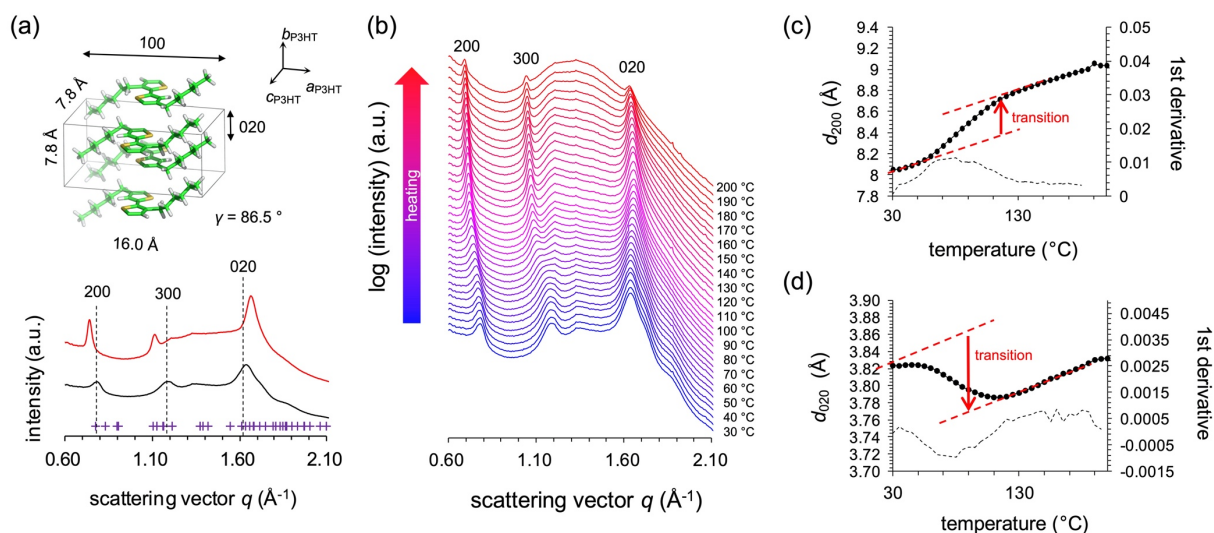


Figure 8. (a) Comparison of WAXS profiles of as-prepared (black) and thermally-annealed (red) bulk P3HT-*b*-AcMal₇ sample. Inset is the widely-accepted unit cell of the P3HT crystal. Reflection positions estimated based on the unit cell are plotted with purple marks in the graph. (b) WAXS profiles of P3HT-*b*-AcMal₇ bulk sample during *in situ* heating process from 30 to 200 °C. Variation of (c) d_{200} and (d) d_{020} as a function of temperature. Black dotted lines in (c) and (d) indicate first derivatives of d_{200} and d_{020} , respectively.

CONCLUSIONS

A structural model of P3HT-*b*-AcMal₇ lamella was proposed based on the space-filling arguments and electron diffraction data. The P3HT and AcMal₇ segments are confined in the lamellae in which the AcMal₇ segments are aligned side-by-side. The P3HT segments are tilted with respect to the lamellae plane and strongly π -stacked with an extended chain conformation in order to attain thermodynamically stable crystalline structure. This distinct molecular arrangement should be

attained as a result of the competition of multiple factors such as segregation strength between P3HT and AcMal₇, strong π - π interaction of P3HT backbones, geometrical mismatch between two blocks, space filling requirement and entropic penalties.

Thermal properties and thermally-induced structural evolution of P3HT-*b*-AcMal₇ have been systematically investigated by DSC, and *in situ* step-wise heating and cooling X-ray scattering analysis comparing with those of P3HT homopolymer. The temperature-dependent *in situ* SAXS experiments revealed that the P3HT-*b*-AcMal₇ exhibits phase-separated lamellar structure in the molten state. Although order-disorder transition of the lamellar phase could not be observed in the experimental temperature range, the P3HT-*b*-AcMal₇ can be considered as a strongly segregated system. The confined crystallization phenomenon of the P3HT block was further corroborated by DSC analyses. The P3HT-*b*-AcMal₇ showed a more complex melting behavior as compared to the P3HT homopolymer. In particular, when the block copolymer was solidified rapidly from the molten state, two endothermic peaks were observed in the heating thermogram. The two melting peaks support the coexistence of two different P3HT phases that are formed through different crystallization processes, *i.e.* (i) metastable crystal formed under the control of kinetic factors and (ii) stable crystal formed under the control of thermodynamic factors. The origin of such a behavior can be attributed to the tethering of P3HT with AcMal₇ which leads to the different chemical and geometrical environments for the P3HT segments (weakly mobile chain-end anchored by AcMal₇, highly crystallizable middle part, and highly mobile free chain-end). Thus, the crystallization of the P3HT segment occurs in the confined space of the lamellar phase where the contribution of tethering effect cannot be avoided. While this study focused on the specific case of P3HT-*b*-AcMal₇, we believe that our results provided new insights into the temperature-dependent self-assembly behavior of the P3HT confined in a phase-separated lamellar structure and hope that it

will be a guide to the better control of hierarchical structures and the more rational design toward the high-performing semiconducting block copolymer systems.

AUTHOR INFORMATION

Corresponding Author

Redouane Borsali – Univ Grenoble Alpes, CERMAV, CNRS, F-38000 Grenoble, France;
ORCID: <https://orcid.org/0000-0002-7245-586X>
Email: borsali@cermav.cnrs.fr

NOTES

The authors declare no competing financial interest.

ACNOWLEDGEMENTS

R.B. would like to gratefully thank the CNRS and Univ Grenoble Alpes for partial financial support in this project, the Advanced Research Center for Green Materials Science and Technology, National Taiwan University (NTU) and Hokkaido University (Laboratory of Polymer Chemistry, Faculty of Engineering) for exchange students and fruitful collaboration. Specifically, R.B. acknowledges partial financial support from SweetMemory International France-Taiwan ANR project (#ANR-14-CE08-0021), Institute Carnot PolyNat ANR (#CARN-025-01), the European Union's Seventh Framework Program (FP7/2007-2013) under grant agreement #603519 and Labex ARCANE (project number #ANR-11-LABX-003). This work was financially supported by the JSPS Grant-in-Aid for Scientific Research (B) (19H02769, T. S.) and the Photo-excitonix Project (Hokkaido University, T. S.). The authors thank the NanoBio-ICMG platform (FR 2607, Grenoble) for granting access to the electron microscopy facility. The WOS detector on

the BM02 beamline at ESRF was funded by Agence Nationale de la Recherche (ANR, France) under the "Investissements d'Avenir" program (grant number #ANR-11-EQPX-0010). We thank Isabelle Morfin for her technical assistance during the experiments at ESRF. Marc Schmutz and Christian Blanck (TEM platform at ICS) are gratefully acknowledged for technical support in TEM.

Supporting Information

The Supporting Information is available free of charge at: XXXX

Synthetic procedures of Br/H-terminated P3HT, ethynyl-functionalized P3HT, and P3HT-*b*-AcMal₇; experimental procedure of the stepwise heating and cooling FT-IR measurement; experimental procedures of the SAXS and WAXS measurements; comparison of the SEC traces of alkyne-P3HT homopolymers synthesized via post-polymerization functionalization method and *in situ* functionalization method; molecular properties of the synthesized block copolymers; ¹H NMR spectra of Br/H-capped P3HT and alkyne-P3HT in CDCl₃; comparison of two P3HT-*b*-AcMal₇ systems synthesized by different synthetic routes; AFM phase image of as cast film of alkyne-P3HT; schematic overview of the P3HT-*b*-AcMal₇ lamellar structure; whole FT-IR absorption spectrum of the P3HT-*b*-AcMal₇ recorded at room temperature and assignments of the absorption bands; FT-IR absorption spectra of alkyne-P3HT in the region of C_β-H out-of-plane deformation during whole heating and cooling process; thermal properties of P3HT-*b*-AcMal₇ and alkyne-P3HT; SAXS profiles of alkyne-P3HT bulk sample in a *q*-range between 0.25 and 0.36 Å⁻¹ taken during in situ heating and cooling process.

REFERENCES

- (1) Segalman, R. A.; McCulloch, B.; Kirmayer, S.; Urban, J. J. Block Copolymers for Organic Optoelectronics. *Macromolecules* **2009**, *42* (23), 9205–9216. <https://doi.org/10.1021/ma901350w>.
- (2) Lee, Y.; Gomez, E. D. Challenges and Opportunities in the Development of Conjugated Block Copolymers for Photovoltaics. *Macromolecules* **2015**, *48* (20), 7385–7395. <https://doi.org/10.1021/acs.macromol.5b00112>.
- (3) Zhang, S.; Qin, Y.; Zhu, J.; Hou, J. Over 14% Efficiency in Polymer Solar Cells Enabled by a Chlorinated Polymer Donor. *Adv. Mater.* **2018**, *30* (20), 1800868. <https://doi.org/10.1002/adma.201800868>.
- (4) Fu, H.; Wang, Z.; Sun, Y. Polymer Donors for High-Performance Non-Fullerene Organic Solar Cells. *Angew. Chemie Int. Ed.* **2019**, *58* (14), 4442–4453. <https://doi.org/10.1002/anie.201806291>.
- (5) Cui, C.; Li, Y. High-performance conjugated polymer donor materials for polymer solar cells with narrow-bandgap nonfullerene acceptors. *Energy Environ. Sci.* **2019**, *12* (11), 3225–3246. <https://doi.org/10.1039/C9EE02531F>.
- (6) Zhang, G.; Zhao, J.; Chow, P. C. Y.; Jiang, K.; Zhang, J.; Zhu, Z.; Zhang, J.; Huang, F.; Yan, H. Nonfullerene Acceptor Molecules for Bulk Heterojunction Organic Solar Cells. *Chem. Rev.* **2018**, *118* (7), 3447–3507. <https://doi.org/10.1021/acs.chemrev.7b00535>.
- (7) Shaw, P. E.; Ruseckas, A.; Samuel, I. D. W. Exciton Diffusion Measurements in Poly(3-hexylthiophene). *Adv. Mater.* **2008**, *20* (18), 3516–3520. <https://doi.org/10.1002/adma.200800982>.
- (8) Liu, J.; Sheina, E.; Kowalewski, T.; McCullough, R. D. Tuning the Electrical Conductivity and Self-Assembly of Regioregular Polythiophene by Block Copolymerization: Nanowire Morphologies in New Di- and Triblock Copolymers. *Angew. Chemie Int. Ed.* **2002**, *41* (2), 329. [https://doi.org/10.1002/1521-3773\(20020118\)41:2<329::AID-ANIE329>3.0.CO;2-M](https://doi.org/10.1002/1521-3773(20020118)41:2<329::AID-ANIE329>3.0.CO;2-M)
- (9) Iovu, M. C.; Zhang, R.; Cooper, J. R.; Smilgies, D. M.; Javier, A. E.; Sheina, E. E.; Kowalewski, T.; McCullough, R. D. Conducting Block Copolymers of Regioregular Poly(3-hexylthiophene) and Poly(methacrylates): Electronic Materials with Variable Conductivities and Degrees of Interfibrillar Order. *Macromol. Rapid Commun.* **2007**, *28* (17), 1816–1824. <https://doi.org/10.1002/marc.200700401>.
- (10) Boudouris, B. W.; Frisbie, C. D.; Hillmyer, M. A. Nanoporous Poly(3-alkylthiophene) Thin Films Generated from Block Copolymer Templates. *Macromolecules* **2008**, *41* (1), 67–75. <https://doi.org/10.1021/ma071626d>.
- (11) Grancharov, G.; Coulembier, O.; Surin, M.; Lazzaroni, R.; Dubois, P. Stereocomplexed Materials Based on Poly(3-hexylthiophene)-*b*-poly(lactide) Block Copolymers: Synthesis by Organic Catalysis, Thermal Properties, and Microscopic Morphology. *Macromolecules* **2010**, *43* (21), 8957–8964. <https://doi.org/10.1021/ma1012336>.

- (12) Lim, H.; Chao, C.-Y.; Su, W.-F. Modulating Crystallinity of Poly(3-hexylthiophene) via Microphase Separation of Poly(3-hexylthiophene)–Polyisoprene Block Copolymers. *Macromolecules* **2015**, *48* (10), 3269–3281. <https://doi.org/10.1021/ma502417w>.
- (13) Kim, H. J.; Paek, K.; Yang, H.; Cho, C.-H.; Kim, J.-S.; Lee, W.; Kim, B. J. Molecular Design of “Graft” Assembly for Ordered Microphase Separation of P3HT-Based Rod–Coil Copolymers. *Macromolecules* **2013**, *46* (21), 8472–8478. <https://doi.org/10.1021/ma401530q>.
- (14) Dai, C.-A.; Yen, W.-C.; Lee, Y.-H.; Ho, C.-C.; Su, W.-F. Facile Synthesis of Well-Defined Block Copolymers Containing Regioregular Poly(3-hexyl thiophene) via Anionic Macroinitiation Method and Their Self-Assembly Behavior. *J. Am. Chem. Soc.* **2007**, *129* (36), 11036–11038. <https://doi.org/10.1021/ja0733991>.
- (15) Verduzco, R.; Botiz, I.; Pickel, D. L.; Kilbey, S. M.; Hong, K.; Dimasi, E.; Darling, S. B. Polythiophene-*block*-polyfluorene and Polythiophene-*block*-poly(fluorene-*co*-benzothiadiazole): Insights into the Self-Assembly of All-Conjugated Block Copolymers. *Macromolecules* **2011**, *44* (3), 530–539. <https://doi.org/10.1021/ma102728z>.
- (16) He, M.; Han, W.; Ge, J.; Yang, Y.; Qiu, F.; Lin, Z. All-conjugated poly(3-alkylthiophene) diblock copolymer-based bulk heterojunction solar cells with controlled molecular organization and nanoscale morphology. *Energy Environ. Sci.* **2011**, *4* (8), 2894. <https://doi.org/10.1039/c1ee01509e>.
- (17) Ho, V.; Boudouris, B. W.; Segalman, R. A. Tuning Polythiophene Crystallization through Systematic Side Chain Functionalization. *Macromolecules* **2010**, *43* (19), 7895–7899. <https://doi.org/10.1021/ma101697m>.
- (18) Ho, V.; Boudouris, B. W.; McCulloch, B. L.; Shuttle, C. G.; Burkhardt, M.; Chabinyc, M. L.; Segalman, R. A. Poly(3-alkylthiophene) Diblock Copolymers with Ordered Microstructures and Continuous Semiconducting Pathways. *J. Am. Chem. Soc.* **2011**, *133* (24), 9270–9273. <https://doi.org/10.1021/ja2035317>.
- (19) Moon, H. C.; Bae, D.; Kim, J. K. Self-Assembly of Poly(3-dodecylthiophene)-*block*-poly(methyl methacrylate) Copolymers Driven by Competition between Microphase Separation and Crystallization. *Macromolecules* **2012**, *45* (12), 5201–5207. <https://doi.org/10.1021/ma300902n>.
- (20) Patel, S. N.; Javier, A. E.; Beers, K. M.; Pople, J. A.; Ho, V.; Segalman, R. A.; Balsara, N. P. Morphology and Thermodynamic Properties of a Copolymer with an Electronically Conducting Block: Poly(3-ethylhexylthiophene)-*block*-poly(ethylene oxide). *Nano Lett.* **2012**, *12* (9), 4901–4906. <https://doi.org/10.1021/nl302454c>.
- (21) Lin, S.-H.; Wu, S.-J.; Ho, C.-C.; Su, W.-F. Rational Design of Versatile Self-Assembly Morphology of Rod–Coil Block Copolymer. *Macromolecules* **2013**, *46* (7), 2725–2732. <https://doi.org/10.1021/ma302220b>.
- (22) Sakai-Otsuka, Y.; Zaioncz, S.; Otsuka, I.; Halila, S.; Rannou, P.; Borsali, R. Self-Assembly of Carbohydrate-*block*-Poly(3-hexylthiophene) Diblock Copolymers into Sub-10 nm Scale Lamellar Structures. *Macromolecules* **2017**, *50* (8), 3365–3376. <https://doi.org/10.1021/acs.macromol.7b00118>.
- (23) Olsen, B. D.; Shah, M.; Ganesan, V.; Segalman, R. A. Universalization of the Phase

- Diagram for a Model Rod–Coil Diblock Copolymer. *Macromolecules* **2008**, *41* (18), 6809–6817. <https://doi.org/10.1021/ma800978c>.
- (24) Poelking, C.; Andrienko, D. Effect of Polymorphism, Regioregularity and Paracrystallinity on Charge Transport in Poly(3-hexylthiophene) [P3HT] Nanofibers. *Macromolecules* **2013**, *46* (22), 8941–8956. <https://doi.org/10.1021/ma4015966>.
 - (25) Steyrlleuthner, R.; Di Pietro, R.; Collins, B. A.; Polzer, F.; Himmelberger, S.; Schubert, M.; Chen, Z.; Zhang, S.; Salleo, A.; Ade, H.; et al. The Role of Regioregularity, Crystallinity, and Chain Orientation on Electron Transport in a High-Mobility n-Type Copolymer. *J. Am. Chem. Soc.* **2014**, *136* (11), 4245–4256. <https://doi.org/10.1021/ja4118736>.
 - (26) Zen, A.; Pflaum, J.; Hirschmann, S.; Zhuang, W.; Jaiser, F.; Asawapirom, U.; Rabe, J. P.; Scherf, U.; Neher, D. Effect of Molecular Weight and Annealing of Poly(3-hexylthiophene)s on the Performance of Organic Field-Effect Transistors. *Adv. Funct. Mater.* **2004**, *14* (8), 757–764. <https://doi.org/10.1002/adfm.200400017>.
 - (27) Brinkmann, M.; Rannou, P. Molecular Weight Dependence of Chain Packing and Semicrystalline Structure in Oriented Films of Regioregular Poly(3-hexylthiophene) Revealed by High-Resolution Transmission Electron Microscopy. *Macromolecules* **2009**, *42* (4), 1125–1130. <https://doi.org/10.1021/ma8023415>.
 - (28) Tremel, K.; Fischer, F. S. U.; Kayunkid, N.; Pietro, R. Di; Tkachov, R.; Kiriya, A.; Neher, D.; Ludwigs, S.; Brinkmann, M. Charge Transport Anisotropy in Highly Oriented Thin Films of the Acceptor Polymer P(NDI2OD-T2). *Adv. Energy Mater.* **2014**, *4* (10), 1301659. <https://doi.org/10.1002/aenm.201301659>.
 - (29) Biniek, L.; Pouget, S.; Djurado, D.; Gonthier, E.; Tremel, K.; Kayunkid, N.; Zaborova, E.; Crespo-Monteiro, N.; Boyron, O.; Leclerc, N.; et al. High-Temperature Rubbing: A Versatile Method to Align π -Conjugated Polymers without Alignment Substrate. *Macromolecules* **2014**, *47* (12), 3871–3879. <https://doi.org/10.1021/ma500762x>.
 - (30) Park, J.; Moon, H. C.; Kim, J. K. Facile synthesis for well-defined A₂B miktoarm star copolymer of poly(3-hexylthiophene) and poly(methyl methacrylate) by the combination of anionic polymerization and click reaction. *J. Polym. Sci. Part A Polym. Chem.* **2013**, *51* (10), 2225–2232. <https://doi.org/10.1002/pola.26604>.
 - (31) Takahashi, Y.; Nishikawa, S. Crystal Structure of Amylose Triacetate I. *Macromolecules* **2003**, *36* (23), 8656–8661. <https://doi.org/10.1021/ma030288n>.
 - (32) Kayunkid, N.; Uttiya, S.; Brinkmann, M. Structural Model of Regioregular Poly(3-hexylthiophene) Obtained by Electron Diffraction Analysis. *Macromolecules* **2010**, *43* (11), 4961–4967. <https://doi.org/10.1021/ma100551m>.
 - (33) Toney, M. F.; Russell, T. P.; Logan, J. A.; Kikuchi, H.; Sands, J. M.; Kumar, S. K. Near-surface alignment of polymers in rubbed films. *Nature* **1995**, *374* (6524), 709–711. <https://doi.org/10.1038/374709a0>.
 - (34) Hartmann, L.; Tremel, K.; Uttiya, S.; Crossland, E.; Ludwigs, S.; Kayunkid, N.; Vergnat, C.; Brinkmann, M. 2D Versus 3D Crystalline Order in Thin Films of Regioregular Poly(3-hexylthiophene) Oriented by Mechanical Rubbing and Epitaxy. *Adv. Funct. Mater.* **2011**, *21* (21), 4047–4057. <https://doi.org/10.1002/adfm.201101139>.
 - (35) Lee, Y.-H.; Yen, W.-C.; Su, W.-F.; Dai, C.-A. Self-assembly and phase transformations of

- π -conjugated block copolymers that bend and twist: from rigid-rod nanowires to highly curvaceous gyroids. *Soft Matter* **2011**, 7 (21), 10429. <https://doi.org/10.1039/c1sm05724c>.
- (36) Lee, J.-Y.; Lin, C.-J.; Lo, C.-T.; Tsai, J.-C.; Chen, W.-C. Synthesis, Morphology, and Field-Effect Transistor Characteristics of Crystalline Diblock Copolymers Consisted of Poly(3-hexylthiophene) and Syndiotactic Polypropylene. *Macromolecules* **2013**, 46 (8), 3005–3014. <https://doi.org/10.1021/ma400384a>.
- (37) Yazawa, K.; Inoue, Y.; Yamamoto, T.; Asakawa, N. Dynamic Structure of Regioregulated Poly(alkylthiophene)s. *J. Phys. Chem. B* **2008**, 112 (37), 11580–11585. <https://doi.org/10.1021/jp801972a>.
- (38) He, W.-N.; Xu, J.-T. Crystallization assisted self-assembly of semicrystalline block copolymers. *Prog. Polym. Sci.* **2012**, 37 (10), 1350–1400. <https://doi.org/10.1016/j.progpolymsci.2012.05.002>.
- (39) Sakamoto, N.; Hashimoto, T. Order-Disorder Transition of Low Molecular Weight Polystyrene-*block*-Polyisoprene. 1. SAXS Analysis of Two Characteristic Temperatures. *Macromolecules* **1995**, 28 (20), 6825–6834. <https://doi.org/10.1021/ma00124a018>.
- (40) Alexiadis, O.; Mavrantzas, V. G. All-Atom Molecular Dynamics Simulation of Temperature Effects on the Structural, Thermodynamic, and Packing Properties of the Pure Amorphous and Pure Crystalline Phases of Regioregular P3HT. *Macromolecules* **2013**, 46 (6), 2450–2467. <https://doi.org/10.1021/ma302211g>.
- (41) Joshi, S.; Grigorian, S.; Pietsch, U.; Pingel, P.; Zen, A.; Neher, D.; Scherf, U. Thickness Dependence of the Crystalline Structure and Hole Mobility in Thin Films of Low Molecular Weight Poly(3-hexylthiophene). *Macromolecules* **2008**, 41 (18), 6800–6808. <https://doi.org/10.1021/ma702802x>.
- (42) Joshi, S.; Pingel, P.; Grigorian, S.; Panzner, T.; Pietsch, U.; Neher, D.; Forster, M.; Scherf, U. Bimodal Temperature Behavior of Structure and Mobility in High Molecular Weight P3HT Thin Films. *Macromolecules* **2009**, 42 (13), 4651–4660. <https://doi.org/10.1021/ma900021w>.
- (43) Grigorian, S.; Joshi, S.; Pietsch, U. Temperature-dependent structural properties of P3HT films. *IOP Conf. Ser. Mater. Sci. Eng.* **2010**, 14, 012007. <https://doi.org/10.1088/1757-899X/14/1/012007>.

Supporting Information

Competing Molecular Packing of Blocks in Lamella-forming Carbohydrate-*block*-Poly(3-hexylthiophene) Copolymer

Yoko Sakai-Otsuka,¹ Yoshiharu Nishiyama,¹ Jean-Luc Putaux,¹ Martin Brinkmann,²

Toshifumi Satoh,³ Wen-Chang Chen,⁴ and Redouane Borsali^{1}*

1) Univ Grenoble Alpes, CERMAV, CNRS, F-38000 Grenoble, France

2) Université de Strasbourg, CNRS, ICS UPR 22, F-67000 Strasbourg, France

3) Laboratory of Polymer Chemistry, Division of Applied Chemistry, Faculty of Engineering, Hokkaido University, N13W8, Kita-ku, Sapporo 060-8628, Japan.

4) Advanced Research Center for Green Materials Science and Technology,

National Taiwan University, Taipei 10617, Taiwan

Materials

Maltoheptaose was purchased from Nagase & Co. Ltd. (Japan) and all other reagents were purchased from Sigma-Aldrich and used as received without further purification unless otherwise noted. THF was refluxed and distilled from sodium benzophenone ketyl prior to use to ensure water, oxygen, and peroxide-free state. Lithium chloride (LiCl) was dried *in vacuo* at 140 °C before use. 2, 5-Dibromo-3-hexylthiophene, 1-hexene, and triethylamine were stirred overnight over CaH₂ and distilled prior to use.

Synthesis of Br/H-terminated P3HT

The Br/H-terminated P3HT was synthesized by well-established reported procedure. In a dry 100 mL Schlenk flask, LiCl (1.23 g, 29.1 mmol, 26 equiv.) was introduced and dissolved in freshly distilled dry THF (56 mL). The solution was stirred at room temperature until LiCl was completely dissolved. Then 2, 5-dibromo-3-hexylthiophene (6.0 mL, 28.0 mmol, 25 equiv.) and *tert*-butylmagnesium chloride (13.5 mL, 2.7 mmol, 24 equiv.) were transferred to the flask via syringe under an argon atmosphere and stirred at room temperature overnight in order to complete the metal-halogen exchange reaction. In another dry 500 mL Schlenk flask, Ni (dppp) Cl₂ (0.59 g, 1.1 mmol, 1 equiv.) was added and flame dried, and then 200 mL of dry THF was added. The activated Grignard monomer solution was transferred into a 500 mL Schlenk flask using a cannula and stirred for 30 min at room temperature. 5N HCl was added to the reaction mixture to quench the reaction, and the mixture was stirred for 30 min and then poured into cold methanol. The precipitate was fractionated by successive Soxhlet extraction by using MeOH, Hexane, and DCM. DCM fraction was collected for subsequent reaction. After removal of the solvent, the product was re-solved in THF and precipitated into cold MeOH and dried under reduced pressure to afford Br/H-capped P3HT as a purple solid (yield: 59 %). ¹H NMR (400 MHz, CDCl₃): δ (ppm): 7.06-6.80 (m, aromatic), 2.83-2.48 (m, α -CH₂), 1.71 (m, β -CH₂), 1.48-1.34 (m, -CH₂-CH₂-CH₂-CH₃), 0.92 (br, -CH₃).

Synthesis of ethynyl-functionalized P3HT

The Br/H-terminated P3HT (1.1 g, 0.27 mmol, 1 equiv.), $\text{Pd}_2(\text{dba})_3$ (15 mg, 0.016 mmol, 0.06 equiv.), and $\text{Pd}(\text{P}(\text{t-Bu})_3)_2$ (22 mg, 0.042 mmol, 0.16 equiv.) were added to a flask and dissolved in dry THF (160 mL) under argon. Ethynyltributylstannaane (2.6 g, 8.2×10^{-3} mol, 31 equiv.) was added to the flask and the mixture was stirred at room temperature for 24 h under an argon atmosphere. The mixture was then precipitated into cold methanol to give mono-ethynyl-functionalized P3HT as a dark purple solid (yield: 62 %). ^1H NMR (400 MHz, CDCl_3): δ (ppm): 7.05-6.85 (m, aromatic), 3.53 (s, $-\text{C}\equiv\text{C}-\text{H}$), 2.84-2.50 (m, $\alpha\text{-CH}_2$), 1.71 (m, $\beta\text{-CH}_2$), 1.48-1.34 (m, $-\text{CH}_2\text{-CH}_2\text{-CH}_2\text{-CH}_3$), 0.92 (br, $-\text{CH}_3$). SEC: $M_w = 6210 \text{ g mol}^{-1}$, $M_n = 5670 \text{ g mol}^{-1}$, $D = 1.07$.

Synthesis of poly (3-hexylthiophene)-*b*-peracetylated maltoheptaose (P3HT-*b*-AcMal₇)

In a two-neck round-bottom flask (flask 1), AcMal₇-N₃ (0.86 g, 0.4 mmol, 1.5 equiv.) and PMDETA (85 μL , 0.4 mmol, 1.5 equiv.) were dissolved in THF (10 mL), degassed by bubbling with argon for 5 min and stirred at room temperature. In a second two-neck round-bottom flask (flask 2), alkyne-P3HT (1.00 g, 0.3 mmol, 1 equiv.) and CuBr (0.06 g, 0.4 mmol, 1.5 equiv.) were dissolved in THF (90 mL), degassed by bubbling with argon for 5 min and stirred at room temperature. The content of flask 1 was transferred to flask 2 via cannula under argon atmosphere. The reaction mixture was stirred at room temperature for 4h until the SEC traces showed complete disappearance of the peak of starting material. The solution was passed through a neutral alumina column to remove copper salt. After concentration, the product was recovered by precipitation in cold acetone and dried under reduced pressure to yield the P3HT-*b*-AcMal₇ block copolymer as a purple solid (1.17 g, 75 %). ^1H -NMR (400 MHz, CDCl_3): δ (ppm): 7.77 (s, triazole), 7.06-6.80 (m, aromatic), 5.96 – 3.87 (m, sugar), 2.90-2.48 (m, $\alpha\text{-CH}_2$), 2.20 – 1.98 (m, CH_3 acetyl group), 1.71 (m, $\beta\text{-CH}_2$), 1.54-1.15 (m, $-\text{CH}_2\text{-CH}_2\text{-CH}_2\text{-CH}_3$), 0.92 (br, $-\text{CH}_3$). SEC: $M_w = 10110 \text{ g mol}^{-1}$, $M_n = 8190 \text{ g mol}^{-1}$, $D = 1.23$. FTIR (CaF_2): 1750 cm^{-1} ($\text{C}=\text{O}$, esters).

Stepwise Heating and Cooling FT-IR Measurements

The samples for *in situ* FT-IR study on the structural evolution were prepared by drop-casting of the polymers onto a ZnSe window and set on a Pike Technologies heated solid transmission accessory. The sample was heated from room temperature to 210 °C and held at the target temperature for 3 min. The spectra were then recorded at a 2 cm⁻¹ resolution with 4 scans. All processes were performed under a nitrogen flow. The obtained spectra were normalized to the absorption band at 2922 cm⁻¹ corresponding to the CH₂ asymmetric stretching vibration of the hexyl side chain, $\nu_{\text{as}}(\text{CH}_2)$.

SAXS and WAXS Measurements

All samples for SAXS and WAXS measurements were prepared by drop-casting from concentrated polymer solutions onto a PTFE substrate. THF or chloroform was used as a solvent. The polymer solutions were filtered through a 0.45 µm PTFE filter prior to deposit. After complete evaporation of the solvent, about 10 µm-thick films were treated under optional annealing conditions. The bulk samples were then peeled off from the substrate and finely crashed to put into glass capillaries with a diameter of 1.5 mm. The capillaries were sealed with hot-melt adhesive. The experiments were performed on the BM02 beamline D2AM at the European Synchrotron Radiation Facility (ESRF, Grenoble, France). X-rays of 18 keV ($\lambda = 0.6888 \text{ \AA}$) with a spot size of 100 µm were used for all the measurements. Scattering patterns were recorded on two photon-counting pixel detectors (WOS and D5 from imXpad). In case of the stepwise heating and cooling experiments, the samples were heated from room temperature to 230 °C with an interval of 5 or 10 °C using a thermal controller and cooled by simple heat dissipation.

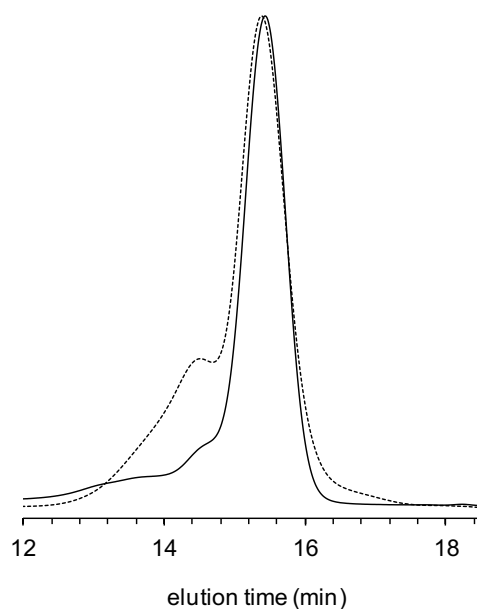


Figure S1. Comparison of the SEC traces of the alkyne-P3HT used in this study which was synthesized via post-polymerization functionalization method (solid line) and the one previously synthesized by *in situ* functionalization method (dotted line).

Table S1. Characterization details of the synthesized carbohydrate-conjugated block copolymers

| entry | sample | method ^a | $M_{n, SEC, P3HT}^b$ (g mol ⁻¹) | $M_{w, SEC, P3HT}^b$ (g mol ⁻¹) | $M_{p, MALDI, P3HT}^c$ (g mol ⁻¹) | \bar{D}^b | ϕ_{P3HT}^d |
|-------|------------------------------------|---------------------------------------|--|--|--|-------------|-----------------|
| 1 | P3HT- <i>b</i> -AcMal ₇ | post-polymerization functionalization | 5670 | 6210 | 3682 | 1.07 | 0.65 |
| 2 | P3HT- <i>b</i> -AcMal ₇ | <i>in situ</i> functionalization | 5330 | 6870 | 3596 | 1.35 | 0.64 |

^a Synthetic methods to prepare alkyne-functionalized P3HT. ^b Number average molecular weight (M_n), weight average molecular weight (M_w), and polydispersity (\bar{D}) determined by SEC in THF based on PS standards. ^c Molecular weight at the peak maximum determined by MALDI-TOF MS. ^d Volume fraction of P3HT in copolymers calculated by using density values 1.16 g cm⁻³ for P3HT and 1.20 g cm⁻³ for AcMal₇.

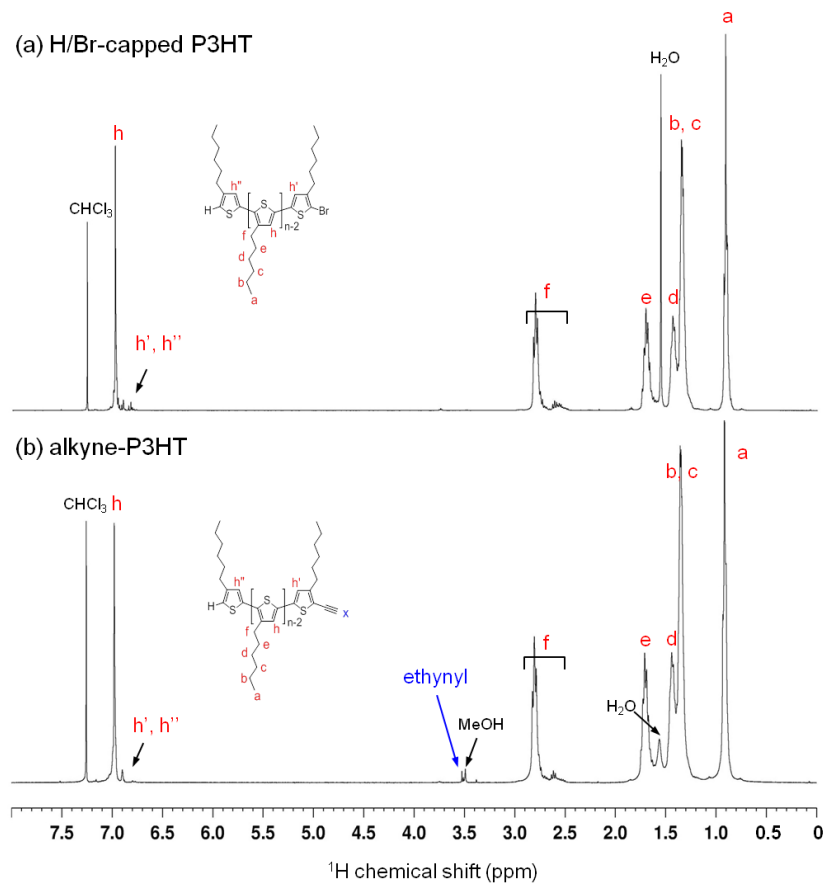
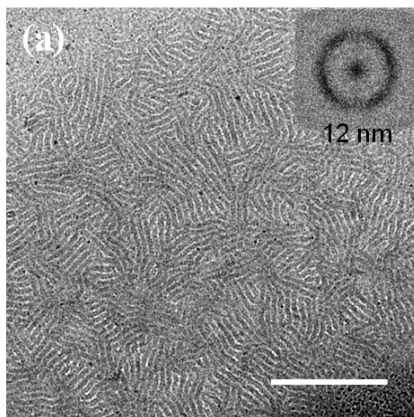


Figure S2. ^1H NMR spectra of (a) Br/H-capped P3HT and (b) alkyne-P3HT in CDCl_3 .

P3HT-*b*-AcMal₇ (entry 1)
[post-polymerization functionalization]



P3HT-*b*-AcMal₇ (entry 2)
[*in situ* functionalization]

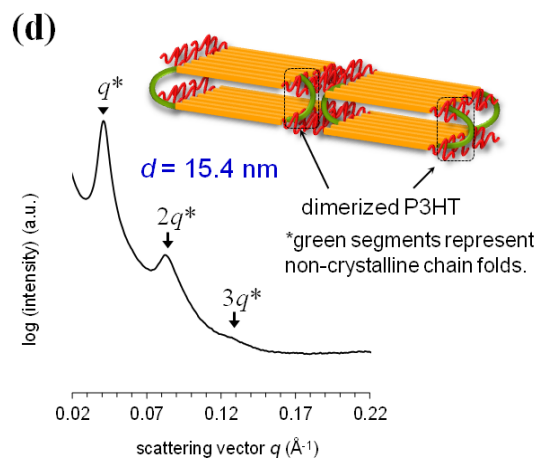
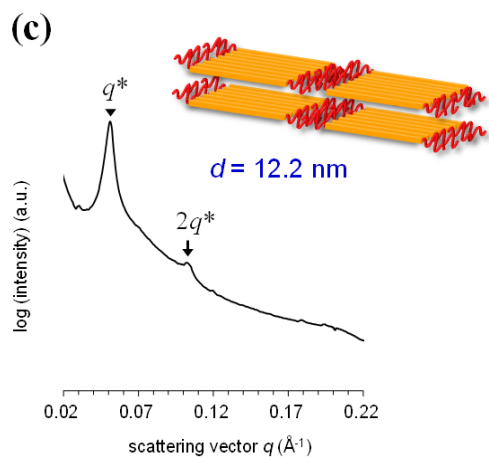
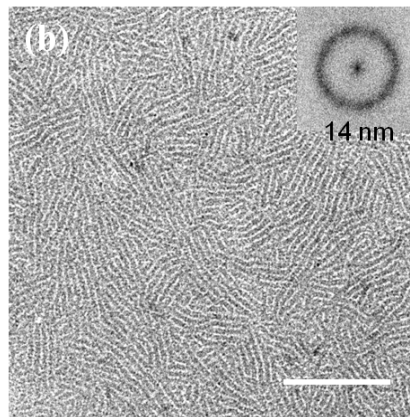


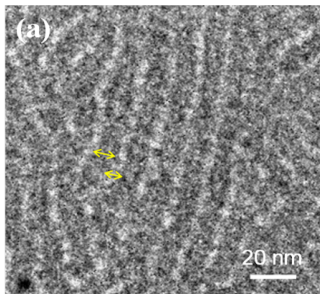
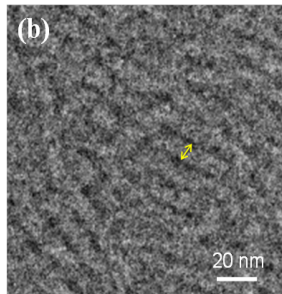
Figure S3. TEM images of (a) P3HT-*b*-AcMal₇ (entry 1 in Table S1) and (b) P3HT-*b*-AcMal₇ (entry 2 in Table S1) thin films obtained after thermal annealing at 220 °C for 10 min. Insets represent fast Fourier transform (FFT) images. Scale bars indicate 200 nm. SAXS profiles of (c) P3HT-*b*-AcMal₇ (entry 1 in Table S1) and (d) P3HT-*b*-AcMal₇ (entry 2 in Table S1) bulk samples obtained after thermal annealing at 220 °C for 10 min.

Table S2. Comparison of two P3HT-*b*-AcMal₇ systems synthesized by different methods.

| | Entry 1: P3HT- <i>b</i> -AcMal ₇ (this study) | Entry 2: P3HT- <i>b</i> -AcMal ₇ (previous study) |
|---|---|---|
| <i>d</i> -spacing | | |
| FFT of TEM image ^a | <i>ca.</i> 12 nm | <i>ca.</i> 14 nm |
| SAXS ^b | 12.2 nm | 15.4 nm |
| characteristics of P3HT block | | |
| end-functionalization method | post-polymerization functionalization | <i>in situ</i> functionalization |
| HT coupled regioregularity ^c | > 94 % | > 95 % |
| bi-ethynyl-functionalized P3HT ^d | 0 % | 7 % |
| dimerized P3HT | poor | rich |
| <i>D</i> _{P3HT} ^e | 1.07 | 1.35 |

^a *d*-spacing determined by Fast Fourier transform(FFT) of TEM image. ^b *d*-spacing determined from primary scattering peak q^* in the corresponding SAXS profiles. ^c Head-to-tail (HT) coupling regioregularity determined by ¹H NMR. ^d The amount of bi-ethynyl-functionalized P3HT determined by MALDI-TOF MS. ^e Polydispersity (*D*) determined by SEC in THF based on PS standards.

Table S3. Experimental structural parameters for P3HT-*b*-AcMal₇ and alkyne-P3HT.

| | | P3HT- <i>b</i> -AcMal ₇ lamellar structure | | | alkyne-P3HT nano fibrils |
|---|-------------------|--|--------------|--------------------------|---|
| | | BCP | P3HT block | AcMal ₇ block | |
| SAXS ^a | | 12.2 nm | – | – | 10.7 nm |
| TEM ^b | FFT | 12.1 nm | – | – | 10.6 nm |
| | visual estimation | 12.1 ± 0.4 nm | 7.1 ± 0.8 nm | 5.0 ± 0.7 nm | 8.7 ± 0.8 nm |
| | |  | | |  |
| | | <ul style="list-style-type: none">➤ dark domain → P3HT➤ bright domain → AcMal₇ | | | <ul style="list-style-type: none">➤ P3HT nano fibrils |
| ^a <i>d</i> -spacings determined from primary scattering peak <i>q</i> [*] in the corresponding SAXS profiles. | | | | | |
| ^b The widths of each domain for the P3HT- <i>b</i> -AcMal ₇ and P3HT nano fibrils were estimated by using inset TEM images (a) and (b), respectively. | | | | | |

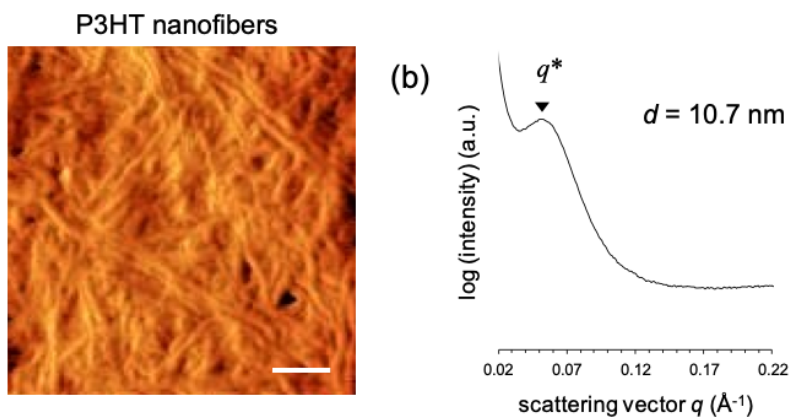


Figure S4. (a) AFM phase image of as cast film of alkyne-P3HT. Scale bars indicate 100 nm (b) SAXS profile of as prepared alkyne-P3HT bulk sample.

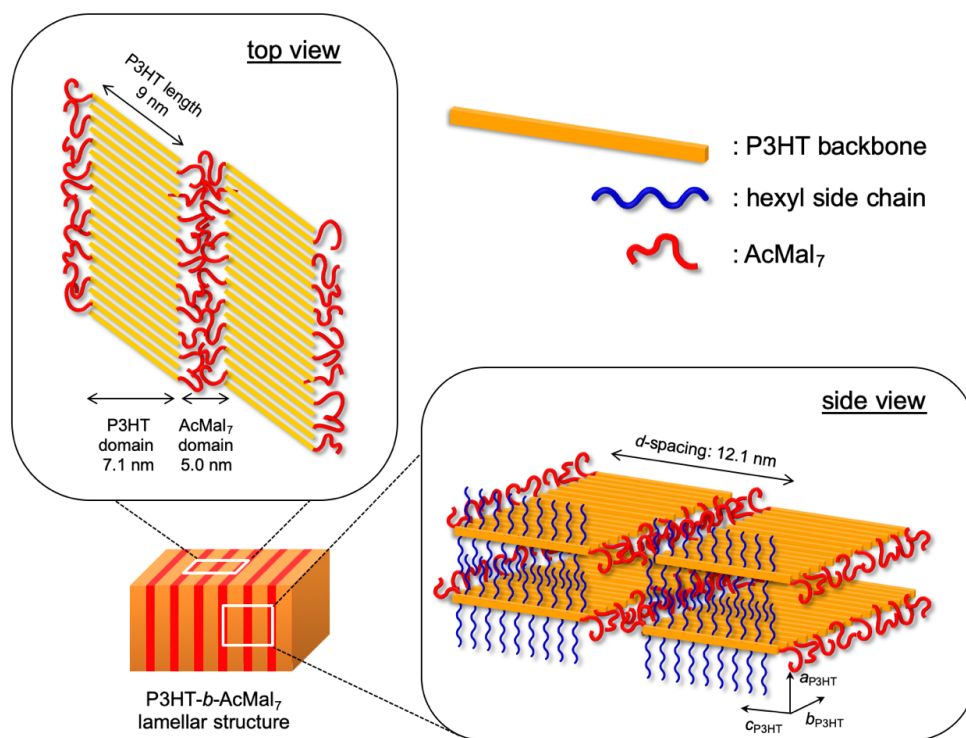


Figure S5. Overall view of the proposed molecular packing model of P3HT-*b*-AcMal₇ lamellar structure, where orange bar, blue and red line represent the P3HT backbone, hexyl side-chain of P3HT, and AcMal₇, respectively.

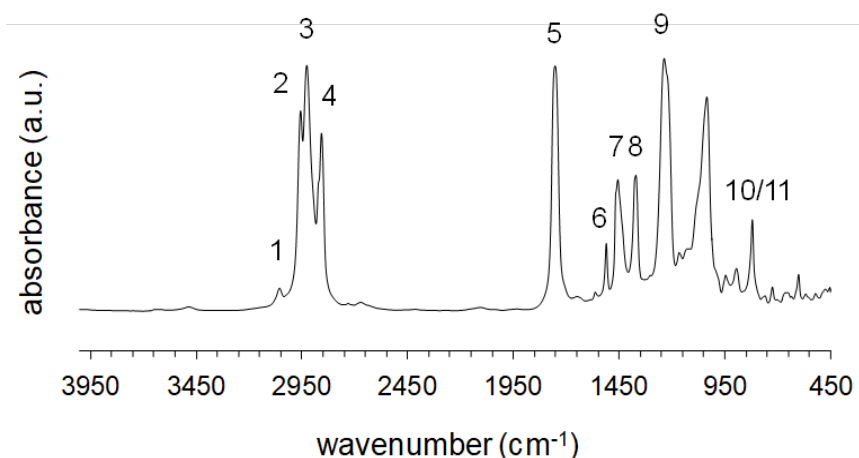


Figure S6. FT-IR absorbance spectra of the P3HT-*b*-AcMal₇ recorded at room temperature.

Table S4. Assignments of FT-IR absorption bands for P3HT-*b*-AcMal₇

| peak code ^a | wavenumber (cm ⁻¹) | related structure | assignments |
|------------------------|-----------------------------------|------------------------------------|---|
| 1 | 3054 | thiophene ring (P3HT) | C _β -H out-of-plane stretching |
| 2 | 2955 | hexyl chain (P3HT) | CH ₃ asymmetric stretching |
| 3 | 2926 | hexyl chain (P3HT) | CH ₂ asymmetric stretching |
| 4 | 2856 | hexyl chain (P3HT) | CH ₂ symmetric stretching |
| 5 | 1753 | carbonyl (AcMal ₇) | C=O stretching |
| 6 | 1510 | thiophene ring (P3HT) | C ₂ =C ₃ , C ₄ =C ₅ symmetric stretching |
| 7 | 1456 | thiophene ring (P3HT) | C ₂ =C ₃ , C ₄ =C ₅ asymmetric stretching |
| 8 | 1371 | acetyl group (AcMal ₇) | C-H (CH ₃) bending |
| | | hexyl chain (P3HT) | C-H (CH ₃) bending |
| 9 | 1237 | acetyl (AcMal ₇) | C-O stretching |
| 10 | 833 | thiophene ring (P3HT) | C _β -H bending in amorphous phase |
| 11 | 820 | thiophene ring (P3HT) | C _β -H bending in crystalline phase |

^a Peak code are shown in Figure S6.

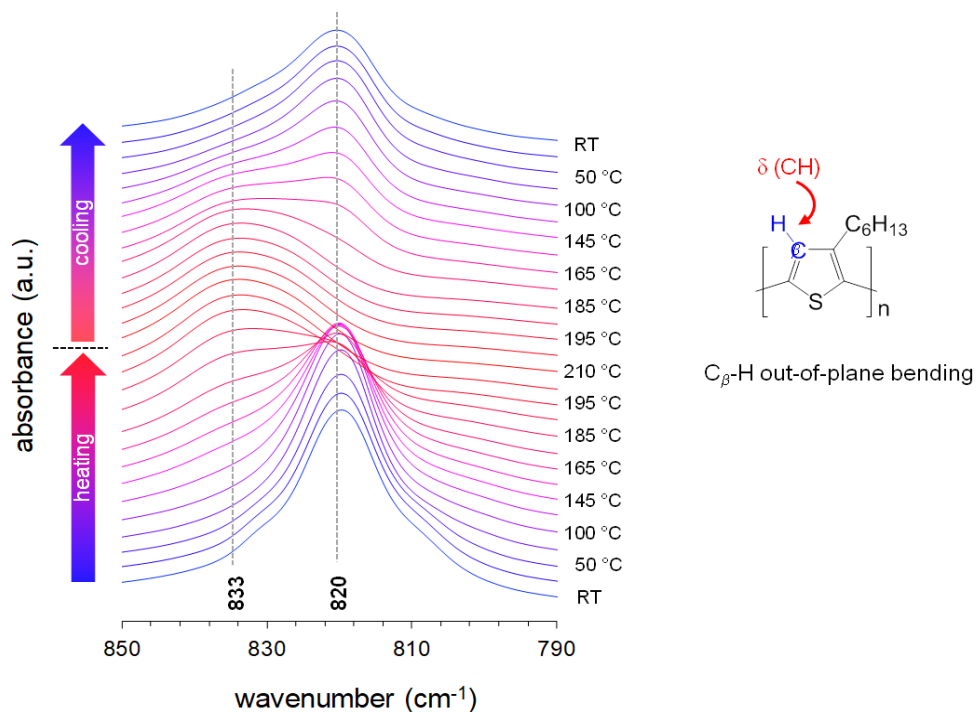


Figure S7. Variation of FT-IR absorption spectra of alkyne-P3HT in the region of C_{β} -H out-of-plane deformation associated with π -stacking mode of thiophene rings during whole heating and cooling process.

Table S5. Thermal properties of P3HT-*b*-AcMal₇ and alkyne-P3HT obtained by DSC analysis

| sample | cooling rate (°C min ⁻¹) | heating cycle | | | |
|------------------------------------|---|---------------|----------|-----------------------------------|-------------------------------|
| | | T_m (°C) | | ΔH_m (J g ⁻¹) | |
| | | 1st peak | 2nd peak | $\Delta H_{m, \text{total}}^a$ | $\Delta H_{m, \text{P3HT}}^b$ |
| P3HT- <i>b</i> -AcMal ₇ | as prepared | 193 | – | – | – |
| | 2 | 194 | – | 12.3 | 18.9 |
| | 10 | 190 | 198 | 11.8 | 18.1 |
| | 20 | 188 | 198 | 11.9 | 18.2 |
| | 30 | 186 | 197 | 11.4 | 17.5 |
| alkyne-P3HT | as prepared | 187 | – | – | – |
| | 2 | 188 | – | 15.5 | 15.5 |
| | 10 | 186 | – | 14.1 | 14.1 |
| | 20 | 185 | – | 13.9 | 13.9 |
| | 30 | 185 | – | 12.9 | 12.9 |

^a The experimental values of total melting enthalpy. ^b Corrected values based on the P3HT weight fraction.

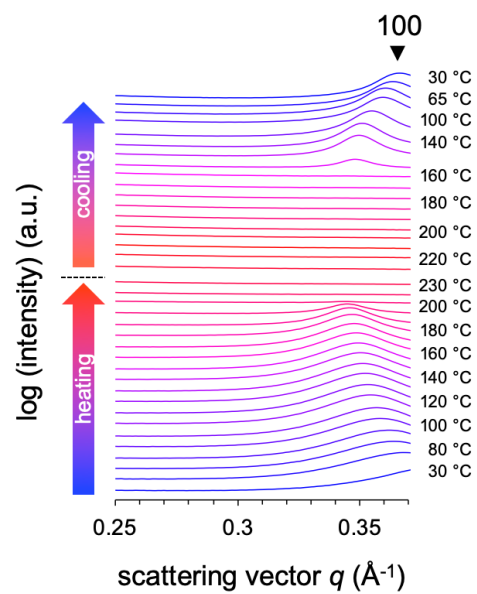


Figure S8. SAXS profiles of alkyne-P3HT bulk sample in a q -range between 0.25 and 0.36 \AA^{-1} taken during *in situ* heating and cooling process